U N I V E R Z I T E T U B E O G R A D U

PUBLIKACIJE

ELEKTROTEHNIČKOG FAKULTETA

SERIJA:

MATEMATIKA I FIZIKA

№ 244 (1969)

BEOGRAD

PUBLIKACIJE ELEKTROTEHNIČKOG FAKULTETA UNIVERZITETA U BEOGRADU
PUBLICATIONS DE LA FACULTÉ D'ÉLECTROTECHNIQUE DE L'UNIVERSITÉ À BELGRADE

SERIJA: MATEMATIKA I FIZIKA — SÉRIE: MATHÉMATIQUES ET PHYSIQUE

Adresser les échanges contre ces *Publications* et toute correspondance à:
Katedra matematike, Elektrotehnički fakultet, Beograd, poštanski fah 816, *Yougoslavie*

PUBLIKACIJE ELEKTROTEHNIČKOG FAKULTETA UNIVERZITETA U BEOGRADU
PUBLICATIONS DE LA FACULTÉ D'ÉLECTROTECHNIQUE DE L'UNIVERSITÉ À BELGRADE

SERIJA: MATEMATIKA I FIZIKA – SÉRIE: MATHÉMATIQUES ET PHYSIQUE

№ 244 (1969)

DYNAMICS OF ELECTRICAL DISCHARGE IN THE GAS MAGNETRON DIODE*

Dobrilo Đ. Tošić

CONTENTS

* Primljeno za štampu 20. novembra 1968. na predlog Branislave Đ. Perović.

0. INTRODUCTION

The magnetron diode consists of a cylindrical cathode surrounded by a cylindrical anode, both of finite dimensions. The system is submitted to an axial magnetic field. The fundamental characteristic of the magnetron diode is the switching action of the magnetic field. Electrons from the cathode, accelerated by the radial electric field, are deflected tangentially by axial magnetic field. Above a critical value of the magnetic field the deflection is so strong that the electrons do not reach the anode, so the anode current is cut off.

The theory of the direct current magnetron was developed in 1921 by A.W. HULL [**1**] and the first approximations were made neglecting the finite dimensions. Since then the behaviour of the charged particles in such geometry has been the subject of permanent consideration of many authors [**2—15**]. The majority of papers dealing with the theory of the vacuum magnetron diode are concerned with the evaluation of the potential distribution and its change with the magnetic field in order to discover the mechanism of the build-up of very high frequency oscillations. All these papers are based on assumed types of electron beams in the magnetron, assumed electron velocity distributions, etc., and an exact theory of the vacuum magnetron diode has not been formulated so far.

It is natural that the analysis becomes incomparably more complicated if we consider the gaseous magnetron diode. Experimental data on the magnetron diode are such that further theoretical work, under the assumption of ideal vacuum, has no practical value. Even under the best laboratory vacua of the order of 10^{-10} torr, the magnetron diode has to be considered as a gaseous tube [**16**] because of the very long electron paths in over-cutoff conditions, which leads to increased equivalent pressure and corresponding increase in the probability of gas ionization.

From the point of view of application, World War II has witnessed tremendous development of the pulsed resonant magnetron, which was the main source of SHF power in radar [**17**]. In the past few years the magnetron diode has been successfully used in the production and measurement of ultra-high vacua [**18—22**]. Because of their diverse properties, magnetron diodes have been used for special applications [**23—25**].

The first attempt to use the gas magnetron diode for the production of protons was made as early as 1934 [**26**]. Two years later a paper describing the production of H_2^+ ions in this geometry was published [**27**]. The ion currents obtained were of the order of microamperes. In 1938 the Soviet investigators SITNIKOV [**28**] and VIGDORCHIK [**29**] attempted the extraction of intense ion beams from the magnetron discharge. After this, for some 20 years, there were no attempts to build ion sources based on the magnetron diode principle.

In 1957 the Ion Physics Laboratory of the Boris Kidrič Institute in Beograd, constructed an electromagnetic isotope separator which initially used a Nier-type ion source. In the same year B. PEROVIĆ [30] started the development of an ion source intended for milliampere currents. Her main interest was directed towards the development of ion sources for electromagnetic separation of stable isotopes. The first results showed that this ion source has certain advantages over other types of ion sources from the point of view of intensity, the high yield of multi-charged ions and the relative ease of production of ions of refractory elements.

The development of ion sources required a detailed knowledge of the characteristic of the gas discharge in the magnetron diode, which is the subject of this dissertation. The very first results have revealed a number of interesting properties of this discharge, related to the action of the axial magnetic field. The fundamental difference between the discharge in the magnetron diode and the discharge in an ordinary diode lies in the fact that the initiation of the intense magnetron discharge occurs at pressures of the order of 10^{-4} torr, which is several orders of magnitudes lower than in the ordinary diode, and is due to the lenthening of the electron paths. The anode current cutoff occurs at a much higher magnetic field than in the vacuum magnetron diode. The inhibited electron transport in the direction of the electric field points to the formation of an intense electron cloud rotating at high speed around the cathode. The question naturally arises as to whether Maxwell distribution of electron velocities will be established, because of the length of the electron paths and the large number of collisions, although the pressure is low. The existence of an intense electron cloud raises the problem of its stability. All these problems have been studied in Chapter 1.

Chapter 2 deals with the problem of the self magnetic field. Intense ion sources use direct heated cathodes with large emission currents. In the measurements of currents emitted from the cathode it was noticed that the anode current can be cut off by increasing the heating current. This was why the influence of the self magnetic field, induced by the heating current, on electron motion in the cylindrical diode was analyzed in detail.

The applications of the gas magnetron diode are described in Chapter 3. Here the main concern is the magnetron ion source and its properties. The same chapter also deals with the application of the gas magnetron diode as an ionization tube of original construction for pressure measurements.

It should be mentioned that this type of discharge in large magnetron structures is of some importance in modern plasma investigations. Under certain conditions a rotating plasma in the magnetron geometry is formed with the hope to achieve high temperatures and densities required for thermonuclear processes [31—33].

* * *

This dissertation contains results of the investigations of the gas magnetron diode and its applications, carried out in the Ion Physics Laboratory of the Boris Kidrič Institute in Beograd since 1958. The dissertation is based on the papers that the author has published by himself and together with his collegues [34—47], and on the recent unpublished work.

The author is much indepted to Prof. B. Dj. Perović for stimulating discussions, many constructive comments and suggestions, to Prof. B. V. Surutka and Prof. D. S. Mitrinović for permanent interest in this work, to D. B. Ilić, Dr B. A. Aničin and Dr R. R. Janić for help in preparing the manuscript.

1. CHARACTERISTICS OF THE GAS MAGNETRON DIODE

Electric discharge in the gas magnetron diode has different characteristics compared with a simple diode. Under the action of an axial magnetic field the electron path lengthens, thus enabling the production of highly-ionized gas. The anode current increases several times compared with a diode without magnetic field, since the electron-neutral collisions lead to the multiplication of electrons. On the other hand, the cathode is intensely bombarded by ions which causes amplification of electron emission and compensation of space charge.

The fundamental characteristic of the vacuum magnetron diode is the switching action of the magnetic field (cutoff). In the gas magnetron diode cutoff occurs at much higher magnetic fields, than in vacuum conditions. At magnetic fields lower than B_c, the gas magnetron behaves like a gas diode without a magnetic field, so that the influence of the magnetic field appears only at over-critical magnetic fields.

The study of the electron motion dynamics has shown that electron transport toward the anode is inhibited by the magnetic field. In the case of high magnetic fields the motion of electrons is reduced to rotation around the cathode, which produces an intense electron cloud.

Due to this complex influence of the magnetic field, the gas magnetron diode posseses particular characteristics, expressed by many effects, which do not exist in a simple diode.

1.1. **Dynamics of electron motion in the magnetron diode**

The behaviour of plasma is determined from the interaction of the plasma particles with themselves and with externally applied electric and magnetic fields. Since we observe a low pressure gas magnetron diode, we shall only consider the electron-neutral interactions and electron motion induced by a radial electric and axial magnetic field. In analyzing the vacuum magnetron diode, in which neutral concentration is low, electron-neutral collisions may be neglected. However, in the case of gas magnetron diode these collisions must be taken into account, because they represent the only mechanism for electron transport from cathode to anode.

1.1.1. *Elementary theory of the magnetron diode*

A schematic diagram of the magnetron diode is given in Fig. 1. The cylindrical anode with radius R has in its axis a hot filament cathode with radius r_0. The system is set up in the axial magnetic field B. The dc positive anode voltage U produces the radial electric field E. We shall consider the electron motion in this crossed--fields system.

Let an electron start from the cathode. At $t=0$, $r=r_0$, $\theta=0$, $z=0$, $u_0=\frac{dr}{dt}$, $v_0=r\frac{d\theta}{dt}$, $w_0=\frac{dz}{dt}$.

The electron moves under the action of the following forces:

radial: $-eE-eBr\frac{d\theta}{dt}$,

tangential: $eB\frac{dr}{dt}$.

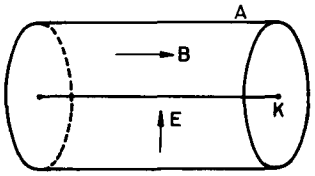

Fig. 1. Magnetron geometry.

Thus, the equations of electron motion are given by

(1) $$m\left[\frac{d^2r}{dt^2}-r\left(\frac{d\theta}{dt}\right)^2\right]=-eE-eBr\frac{d\theta}{dt},$$

(2) $$m\frac{1}{r}\frac{d}{dt}\left(r^2\frac{d\theta}{dt}\right)=eB\frac{dr}{dt},$$

(3) $$m\frac{d^2z}{dt^2}=0.$$

Integrating Eq. (2) in relation to time we obtain

(4) $$r^2\frac{d\theta}{dt}=\frac{1}{2}\frac{e}{m}Br^2+C.$$

For $t=0$ $\quad r_0v_0=\frac{1}{2}eBr_0^2+C.$

Substituting C in Eq. (4), we obtain

(5) $$\frac{d\theta}{dt}=\frac{r_0^2}{r^2}\left(\frac{v_0}{r_0}-\frac{eB}{2m}\right)+\frac{eB}{2m}.$$

If Eq. (5) is substituted in Eq. (1), after integration, we obtain

(6) $$\left(\frac{dr}{dt}\right)^2=2\frac{e}{m}U_r-\left(\frac{e}{2m}\right)^2B^2r^2\left(1-\frac{r_0^2}{r^2}\right)^2-\frac{e}{m}Br_0v_0\left(1-\frac{r_0^2}{r^2}\right)+v_0^2\left(1-\frac{r_0^2}{r^2}\right)+u_0^2,$$

where $U_r=-\int_{r_0}^{r}Edr.$

The radial distance of the electron is maximum when its radial velocity is zero, i.e. when all of its kinetic energy corresponds to the tangential components of the motion. Assuming this to occur at some radius r, from the condition $\frac{dr}{dt}=0$, i.e. from Eq. (6), we get

(7) $$U_r=\frac{e}{8m}B^2r^2\left(1-\frac{r_0^2}{r^2}\right)^2+\left(\frac{Br_0v_0}{2}-\frac{v_0^2}{2e/m}\right)\left(1-\frac{r_0^2}{r^2}\right)-\frac{u_0^2}{2e/m}.$$

Equation (7) may be considerably simplified if the initial electron velocity is neglected. In this case we obtain

(8) $$U_r=\frac{e}{8m}B^2r^2\left(1-\frac{r_0^2}{r^2}\right)^2.$$

If maximum distance of the electron from the cathode is equal to or lower than the anode radius R, the anode current is cut off. The critical case appears at $r=R$, when $U_a=U$, thus Eq. (8) becomes

$$U_a=\frac{e}{8m}B^2R^2\left(1-\frac{r_0^2}{R^2}\right)^2. \tag{9}$$

This is the fundamental relation of the direct current magnetron theory developed by HULL [1].

If the anode voltage U_a is lower than the critical voltage given by Eq. (9), the anode current is cut off (Fig. 2).

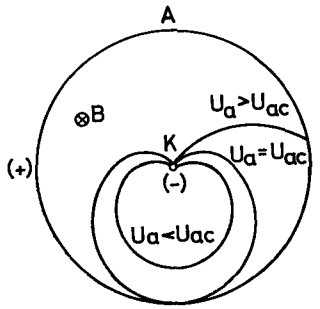

Fig. 2. Electron paths in the vacuum magnetron diode.

Assuming $R_a \gg r_0$, Eq. (9) can be written in a simpler form

$$U_a=\frac{e}{8m}B^2R^2. \tag{10}$$

Introducing the numerical values for e and m, Eq. (10) reduces to

$$U_a=\frac{6.72}{R}\sqrt{U_a}, \tag{11}$$

where U_a is given in volts, R in centimetres and B in gauss.

In calculating Eq. (9) we supposed the electron to start from the cathode, i.e. $U(r_0)=0$, but if the electron starts from some radius r_{k-1} between the cathode and the anode and reaches the maximum distance at some radius r_k, Eq. (8) becomes

$$U_{r_k}-U_{r_{k-1}}=\frac{e}{8m}B^2r_k^2\left(1-\frac{r_{k-1}^2}{r_k^2}\right)^2. \tag{12}$$

This expression can be used to determine the maximum electron energy in case the magnetic field is much higher than critical.

1.1.2. *Dynamics of electron motion in the gas magnetron diode*

When the magnetic field in a vacuum magnetron diode is higher than critical, the anode current is cut off. The electrons practically move in infinite cycloidal orbits around the cathode. In the case of the gas magnetron diode, the probability of electron-neutral collisions is greater because of very long electron paths, which causes the electrons to drift toward the anode, so that the anode current does not cut off (Fig. 3).

The probability of electron-neutral collision is not the same at every point of the cycloidal path. It increases with increasing electron energy, so we have the maximum probability at the maximum distance of the electron from the cathode and we may assume for certain that collisions occur in this part of electron path. We shall presume that the electron loses its total energy in collision, so that it starts from a new radius, which we can call the virtual cathode. It is evident that the number of virtual cathodes n increases with the magnetic field, so that the electron transit to anode being inhibited.

Let two neighbouring virtual cathodes be placed on cylinders $r=r_{k-1}$ and $r=r_k$. Since the magnetic field is much higher than critical, the distance between these cylinders is small with respect to radii r_{k-1} and r_k.

We assume an arbitrary potential distribution

(13) $U(r)=U_a f(r) \qquad (f(r_0)=0,\ f(R)=1).$

Since $r_k-r_{k-1}\ll r_k$, we can write

$$U(r_k)-U(r_{k-1})=(r_k-r_{k-1})\left.\frac{dU}{dr}\right|_{r=r_k}.$$

On the other hand, the condition

$$r_k\cong r_{k-1}=r,$$

gives

$$\left(1-\frac{r_{k-1}^2}{r_k^2}\right)^2\cong\frac{4}{r^2}(r_k-r_{k-1})^2,$$

so that Eq. (12) becomes

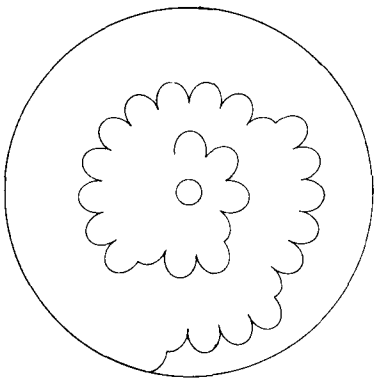

Fig. 3. Electron paths in the gas magnetron diode.

(14) $$\delta(r)=r_k-r_{k-1}=\frac{U_a}{4\dfrac{e}{8m}}\frac{df}{dr}.$$

The mean value of $\delta(r)$ in the interval $[r_0, R]$ is

(15) $$\langle\delta(r)\rangle=\frac{1}{R-r_0}\int_{r_0}^{R}\delta(r)\,dr=\frac{U_a}{4\dfrac{e}{8m}B^2}\frac{1}{R-r_0}[f(R)-f(r_0)].$$

If we use conditions (13) and $R\gg r_0$, Eq. (15) becomes

(16) $$\langle\delta(r)\rangle=\frac{U_a}{4\dfrac{e}{8m}B^2}\frac{1}{R}.$$

Substituting the value for U_a from Eq. (10), the last equation becomes

(17) $$\langle\delta(r)\rangle=\frac{1}{4}\left(\frac{B_c}{B}\right)^2 R.$$

Thus, the number of virtual cathodes n_k is

(18) $$n_k=\frac{R}{\langle\delta(r)\rangle}=4\left(\frac{B}{B_c}\right)^2.$$

This equation is valid only for high magnetic fields ($B/B_c\gg 1$). For example, at $B=10B_c$ we obtain $n_k=400$. If $R=20$ mm, then we have $\langle\delta(r)\rangle=0.05$ mm.

The drift electron velocity is

(19) $$v_d=\langle\delta(r)\rangle\,\nu_c,$$

where ν_c is the collision frequency.

The collision frequency is defined by relation

$$\nu_c = p_0 P_c v, \tag{20}$$

where p_0 is the reduces pressure $\left(p_0 = \frac{273\ ^\circ\mathrm{K}}{T}\, p\right)$, v the electron velocity and P_c the mean number of collisions which the electron suffers when passing through 1 cm of gas at pressure 1 torr.

Naturally, the application of Eq. (20) in our case is a rough approximation. If we observe the electron motion in plasma, the collision frequency is taken to be the mean value, obtained from the electron distribution function.

Since the mean free path of the electron is $l_s = 1/(p_0 P_c)$, it follows that

$$\nu_c = v/l_s\,. \tag{21}$$

For v we can take the electron velocity at its maximum distance. Therefore, we obtain

$$\frac{mv^2}{2} = e\,\langle\delta(r)\rangle\,\frac{du}{dr},$$

i.e.

$$v = \sqrt{\frac{2e\,\langle\delta(r)\rangle\,\dfrac{dU}{dr}}{m}}\,.$$

Using the approximation $\frac{dU}{dr} \cong \frac{U_a}{R}$, the drift velocity is

$$v_d = \langle\delta(r)\rangle\,\frac{v}{l_s} = \sqrt{\frac{2e\,\dfrac{U_a}{R}}{m}}\,\frac{\langle\delta(r)\rangle^{3/2}}{l_s}\,.$$

Since $\langle\delta(r)\rangle = \frac{1}{4}(B_c/B)^2 R$, we can write

$$v_d = \frac{1}{8}\,\frac{R}{l_s}\sqrt{\frac{2eU_a}{m}}\left(\frac{B_c}{B}\right)^3. \tag{22}$$

The square root in Eq. (22) represents the maximum electron velocity v_d' in the cylindrical diode without magnetic field, when the electrons move radially. Thus, we obtain

$$\frac{v_d}{v_d'} = \frac{R_a}{8\,l_s\left(\dfrac{B}{B_c}\right)^3}\,. \tag{23}$$

From equation (23) it is seen that the electron drift velocity is inversely proportional to the cube of the magnetic field.

Beside the radial motion, the electrons move in the tangential direction. The tangential velocity is defined by

$$v_\theta = \frac{E}{B}\,. \tag{24}$$

Assuming the potential distribution to be linear, i.e. $E=U_a/R$, we obtain

$$v_\theta = \frac{U_a}{RB}. \tag{25}$$

For the typical experimental conditions: $U_a=$ 100 V, R=1.9 cm, $B=10B_c$, $B_c=$ 35 Gs, $p=10^{-4}$ torr (argon), the components of the electron velocity are

$$v = 30 \text{ m/sec}, \quad v = 1.5 \cdot 10^6 \text{ m/sec}.$$

It can be concluded that at high magnetic fields ($B \gg B_c$), the electron motion reduces to rotation around the cathode. This fact indicates the existence of an intense rotating electron cloud, which was confirmed experimentally.

1.2. Static characteristics of the gas magnetron diode

1.2.1. *Experimental arrangement*

The cylindrical magnetron diode with power supply and the measuring system is shown in Fig. 4. A 90 mm long anode with a radius of 19 mm, fitted with a tungsten cathode 1 mm in diameter, is placed in the axial magnetic field.

The supply parameters are:

a) filament heating current (dc or ac) 0—50 A,

b) anode voltage 0—600 V,

c) anode current 0—6A,

d) magnetic field 0—800 Gs.

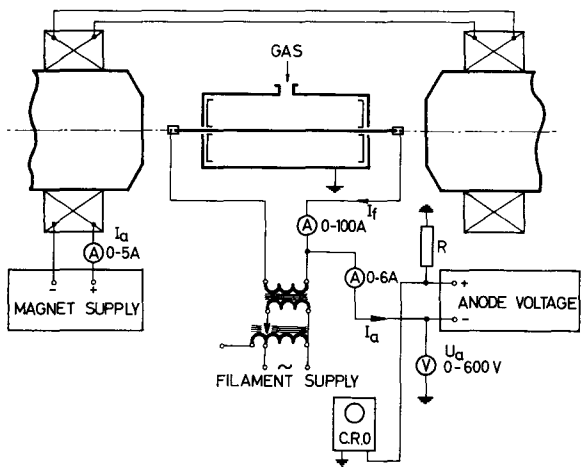

Fig. 4. Circuit for measuring diode characteristics.

The static diode characteristics are obtained by electrical measurement of the filament heating current, anode voltage and anode current. The intensity of the axial magnetic field is determined by measuring the electromagnet current. The gas is introduced in the diode through a needle valve. The pressure is not measu-

red in the diode but in the vacuum chamber, so that the pressure in the diode is estimated. Argon was used in all measurements.

1.2.2. *Characteristics of the vacuum magnetron diode*

The electron emission current as a function of the filament heating current for different values of anode voltage ($B=0$) has a typical diode characteristic (Fig. 5). In the interval $I_f = 40$—45 A all curves are joined together because the electron emission is not limited by space charge as in the case of higher I_f.

The dependence of the anode current on the magnetic field is shown in Fig. 6. The anode current cutoff is not so sharp as predicted by the theory. The measured values of the critical magnetic field B_c are found to be higher than the theoretical values (Fig. 9). The broadening of this characteristic can be mainly attributed to the influence of the filament heating current (Chapter 2) and to additional gas ionization.

The dependence of the anode current on the axial magnetic field for different filament heating currents is given in Fig. 7. At higher I_f the

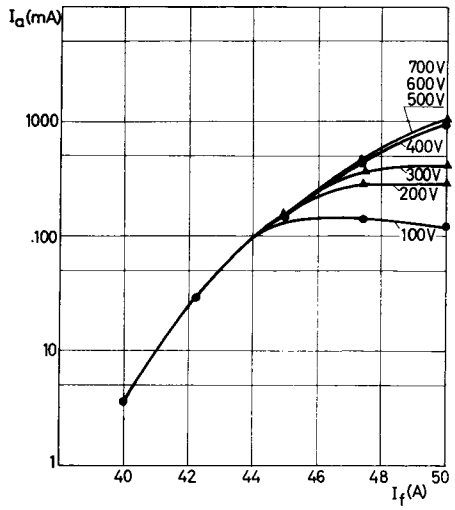

Fig. 5. Electron emission current vs. cathode heating current for different values of anode voltage ($p=5 \cdot 10^{-5}$ torr).

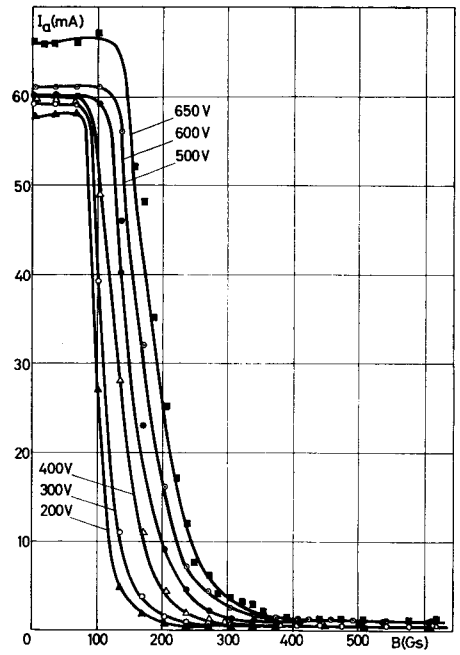

Fig. 6. Anode current vs. magnetic field for different values of anode voltage ($p=5 \cdot 10^{-5}$ torr, I =45 A).

characteristics are the same because of the space charge effect. The curves are presented in semilog plot from which it is obvious that the anode current appears at higher magnetic fields.

1.2.3. *Characteristics of the gas magnetron diode*

When in the magnetron diode gas pressure increases, anode current cutoff does not appear at the over-critical magnetic field, but intense gas discharge starts. Anode current rapidly increases near the critical magnetic field B_{c1}, then remains

almost constant and at some higher magnetic field sharply decreases Fig. 8. This new cutoff magnetic field, B_{c3}, is many times higher than that for the vacuum diode B_{c1}. For the conditions under which the curves in Fig. 8 are obtained the magnetic fields B_{c1} and B_{c3} are

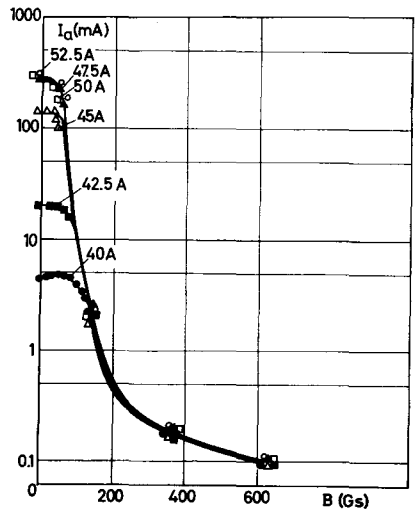

Fig. 7. Anode current vs. axial magnetic field for different values of cathode heating current (U_a=200 V, p=5 · 10^{-5} torr, B_c= 55 Gs).

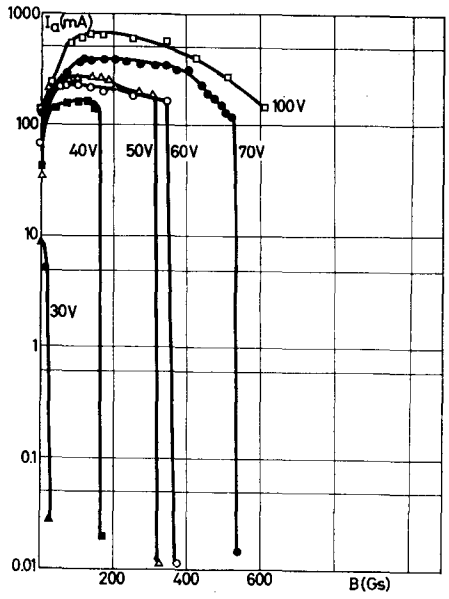

Fig. 8. Anode current vs. axial magnetic field for different values of anode voltage (I_f= 50 A, p=7 · 10^{-4} torr).

U_a	B_{c1} (vacuum)	B_{c3}(gas)
50 V	27 Gs	310 Gs
100 V	38 Gs	610 Gs

The dependence of the cutoff magnetic field on U_a for the vacuum and gas diode is linear (Fig. 9).

From the characteristics given in Fig. 10, where we show the dependence of I_a on B for various filament heating currents, it can be concluded that the cutoff magnetic field B_{c3} increases with increasing anode current. A possible explanation is that there is increasing gas pressure in an intense magnetron gas diode, because strong cathode sputtering appears which results in pressure increase. However, B_{c3} slightly varies with gas pressure (Fig. 11).

This effect points out a new presumption. Namely, from electron motion

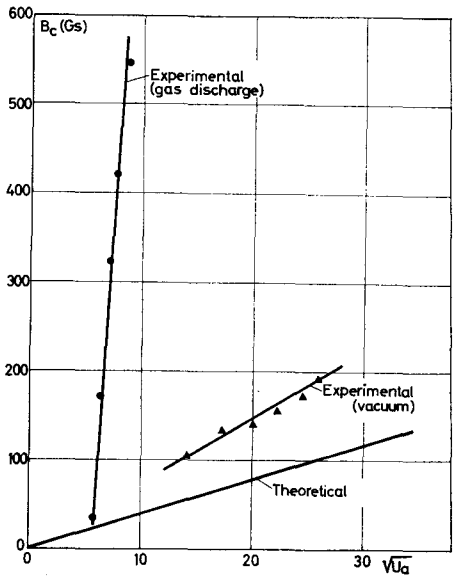

Fig. 9. Cutoff magnetic field as a function of anode voltage.

analysis we have concluded that the tangential electron velocity is much greater than the radial velocity, so that an intense rotating cloud of electrons appears [**16, 48, 49**], even though the magnetron diode is submitted to low pressure. This rotating cloud induces a magnetic field opposite to the initial magnetic field, which naturally increases the cutoff magnetic field.

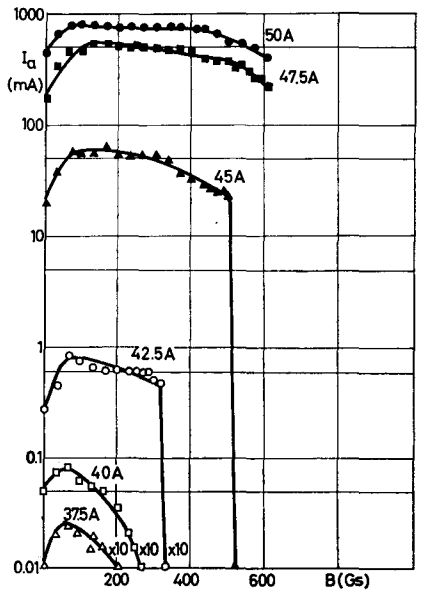

Fig. 10. Anode current vs. axial magnetic field for different values of cathode heating current (U_a= 70 V, p=6 · 10^{-4} torr, B_c= 32 Gs).

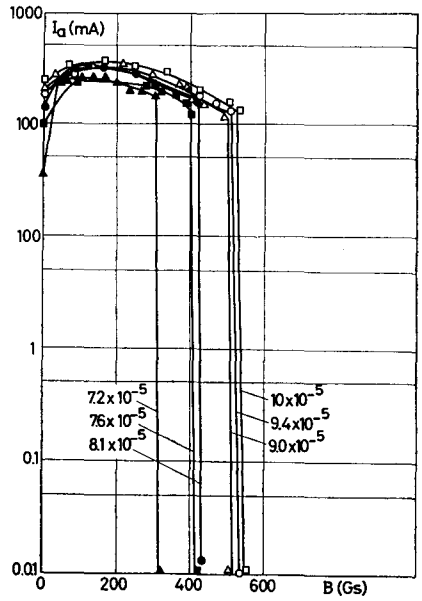

Fig. 11. Anode current vs. axial magnetic field for different values of gas pressure (U_a = 50 V, I_f= 50 A, B_c= 27 Gs).

1.2.4. *Measurements of electron temperature and density*

Electron temperature and density represent the most important characteristics of gas discharge plasma. The use of the Langmuir probes in the determination of these parameters is the simplest experimental method. However, if we investigate a magnetized plasma, the use of the probes is limited to a relatively narrow interval of electron temperatures and densities. If the electron Larmor radius ρ_e is much larger than the Debye radius λ_D, then the probe current density is

$$j_e = \frac{1}{4} n_e e v_e \left(\frac{\pi}{\omega_b \tau}\right) \exp\left(-\frac{eV}{kT_e}\right), \tag{26}$$

where $\omega_b = eB/m$ is the cyclotron frequency and τ the mean collision time for electrons. As can be seen, the magnetic field reduces the electron flux to the probe. A plot of $\log j_e$ against the probe potential V gives a straight line, from which we obtain the electron temperature.

The application of the Langmuir probes is possible if $\tau_e \geqslant 10\lambda_D$, where

$$\rho_e = \frac{m}{eB}\left(\frac{8kT_e}{\pi m}\right)^{1/2}, \quad \lambda_D = 6{,}9\left(\frac{T_e}{n_e}\right)^{1/2}. \tag{27}$$

It is known that the Langmuir probes are used in some configurations similar to magnetron geometry [**50**, **51**], but not in the magnetron diode. In our experiment we measured T_e and n_e in intense magnetron gas discharge in conditions of high magnetic fields ($B \gg B_c$).

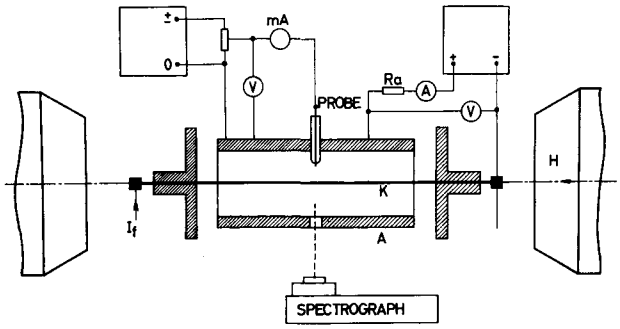

Fig. 12. Circuit for probe measurements.

A schematic diagram of the magnetron diode and the measuring system is given in Fig. 12. The diode dimensions are: $2R=38$ mm, $l=90$ mm, $2r_0=1$ mm. The maximum magnetic field is 500 Gs. The electron temperature and density are measured with the Langmuir probe (2 mm long and 0.5 mm in diameter) placed in the central region of the diode — 5 mm from the anode. The experiment was carried out with low pressure argon plasma. A typical probe characteristic is given in Fig. 13. Under normal working conditions ($p=10^{-3}$ torr, $I_a=1-3$ A, $B=250-500$ Gs) the electron temperature was in the range of 25.000—44.000 °K and density from $8.5\cdot10^{10}$—$3.6\cdot10^{11}$ cm^{-3}. The ratio between the Larmor and Debye radii was greater than 10, so the results were accepted to be sufficiently accurate.

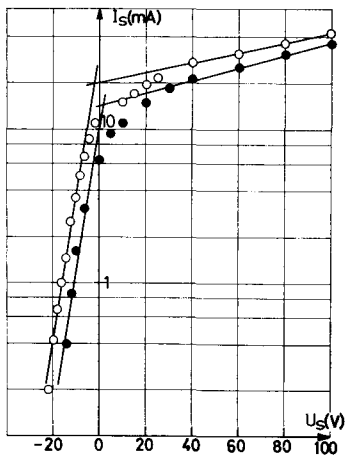

Fig. 13. Typical probe characteristic.

Electron temperature decreases with anode current, and n_e increases as

$$n_e = 0{,}82\cdot10^{11} I_a \text{ cm}^{-3}/A,$$

while T_e and n_e remain almost constant with the magnetic field. The results are given in Table I.

TABLE I

Dependence of the electron temperature and electron density on magnetic field and discharge current

I_a (A)	B (Gs)	T_e (°K)	n (cm^{-3})
1	250	44000	$8.5\cdot10^{10}$
1	500	40000	$1.0\cdot10^{11}$
2	250	30000	$2.8\cdot10^{11}$
2	500	30000	$1.5\cdot10^{11}$
3	250	25000	$3.6\cdot10^{11}$
3	500	25000	$2.5\cdot10^{11}$

1.3. **Dynamic characteristics**

1.3.1. *Oscillations in the gas magnetron diode*

One of the characteristics of plasma state is the appearance of spontaneously and externally induced oscillations and instabilities. These oscillations can be separated into two groups: the first one is in the range up to a few Mc/s and the second one in the μ-wave region. The amplitudes of these oscillations may be very large, which indicates the existence of strong collective processes. In case the electron mean free path is of the order of tube dimension, low frequency oscillations may be excited.

A fundamental property of the crossed-fields discharge is the excitation of a broad spectrum of instabilities. Magnetron gas discharge is characterized by incoherent noise and by coherent sinusoidal oscillations.

Coherent oscillations in cold cathode crossed-field discharge were reported by many authors. Most of them investigated the Penning geometry at pressures higher than 10^{-6} torr [**52—56**]. Low frequency oscillations (500 c/s — 100 kc/s) were observed in an inverted magnetron at 10^{-8} — 10^{-4} torr [**57**]. The frequency of these oscillations was proportional to the ratio of U_a/B. Something similar was noticed in the Penning discharge at $5 \cdot 10^{-4}$ — $4 \cdot 10^{-3}$ torr [**58**]. Coherent oscillations were noticed in cold cathode magnetron discharge at high vacuum (10^{-10}—10^{-6} torr) [**16**], and a linear dependence $f \sim U_a/B$ was also reported.

The dependence of anode current on the axial magnetic field is the main characteristic of the magnetron diode. An idealized characteristic of this type is shown in Fig. 14. When the magnetic field value is B_{c_1} (electron cutoff in the vacuum magnetron), discharge initiates and the anode current increases several times. When the magnetic field increases, the variation of the anode current is negligible. For $B = B_{c_3}$ we have a new discontinuance, i.e. gas discharge ceases and the anode current goes to zero. However, if the magnetic field decreases continually, discharge is set up again at the magnetic field B_{c_2}, which is lower than B_{c_3}. The region between B_{c_2} and B_{c_3} has an unstable character and beside the typical noise, one can detect pure sinusoidal oscillations in the frequency range 0.3—1 Mc/s.

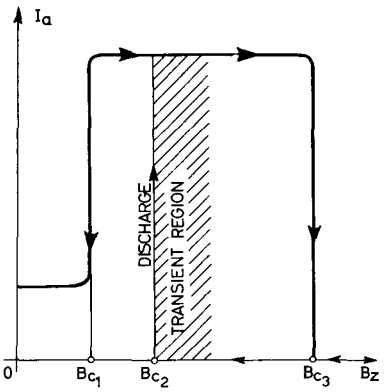

Fig. 14. Idealized characteristic of the gas magnetron diode $I_a(B)$.

The volt-ampere characteristics in the unstable region for different magnetic fields (50—150 Gs) and gas pressures ($4 \cdot 10^{-5}$— $1 \cdot 10^{-4}$ torr) are shown in Figs. 15—17. The anode current is relatively small, because we measure in the region where there is no intense discharge. The numbers against the experimental points indicate the frequency of the oscillations in kc/s. It is seen that the region in which pure sinusoidal oscillations occur is the widest at the pressure $4 \cdot 10^{-5}$ torr. With increasing pressure, this region becomes narrower so that at the pressure of $1.2 \cdot 10^{-4}$ torr no sinusoidal oscillations can be detected.

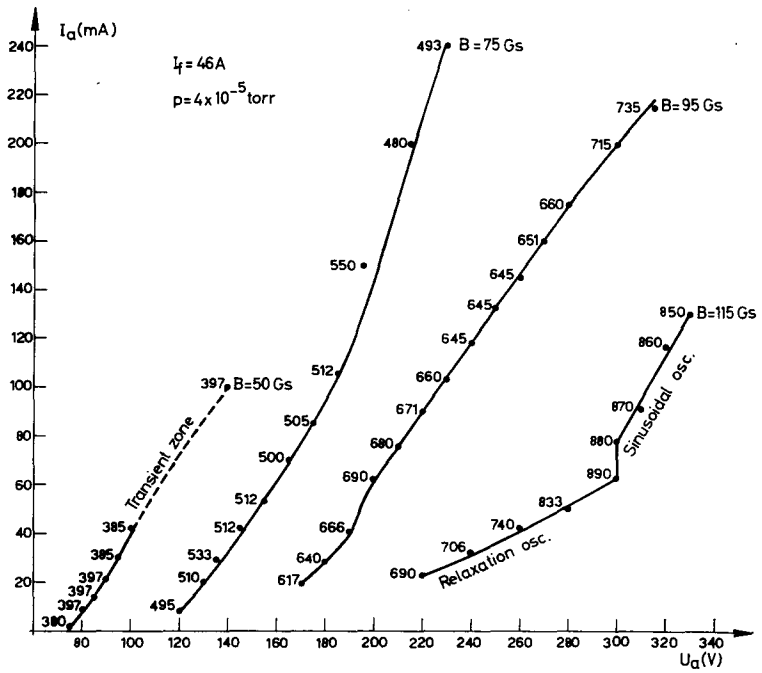

Fig. 15. Volt-ampere characteristic for $p=4 \cdot 10^{-5}$ torr.

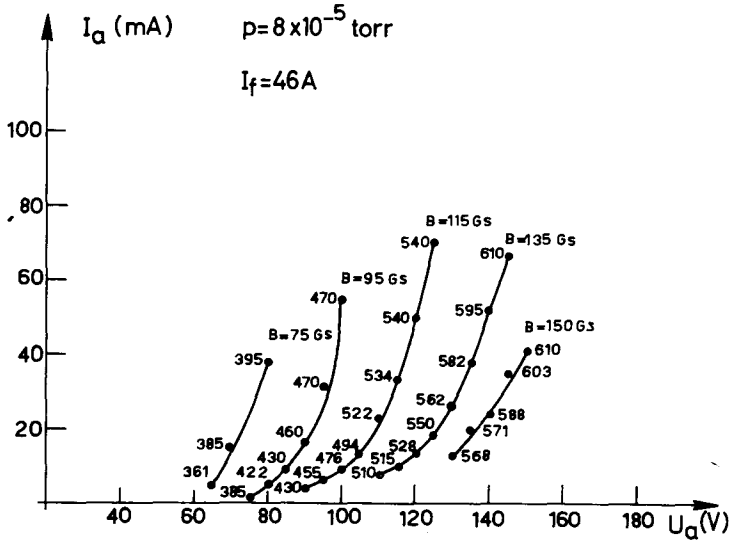

Fig. 16. Volt-ampere characteristic for $p=8 \cdot 10^{-5}$ torr.

The dependence of the frequency of oscillations on the anode current at different magnetic fields is shown in Fig. 18. Up to a certain value of the anode current, the frequency is proportional to $I_a^{1/2}$. For larger values of I_a the curve deviates from this type of dependence, and has some type of frequency saturation.

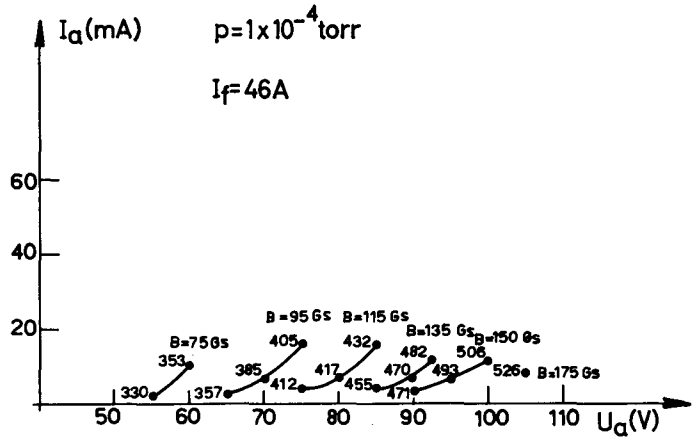

Fig. 17. Volt-ampere characteristic for $p=1 \cdot 10^{-4}$ torr.

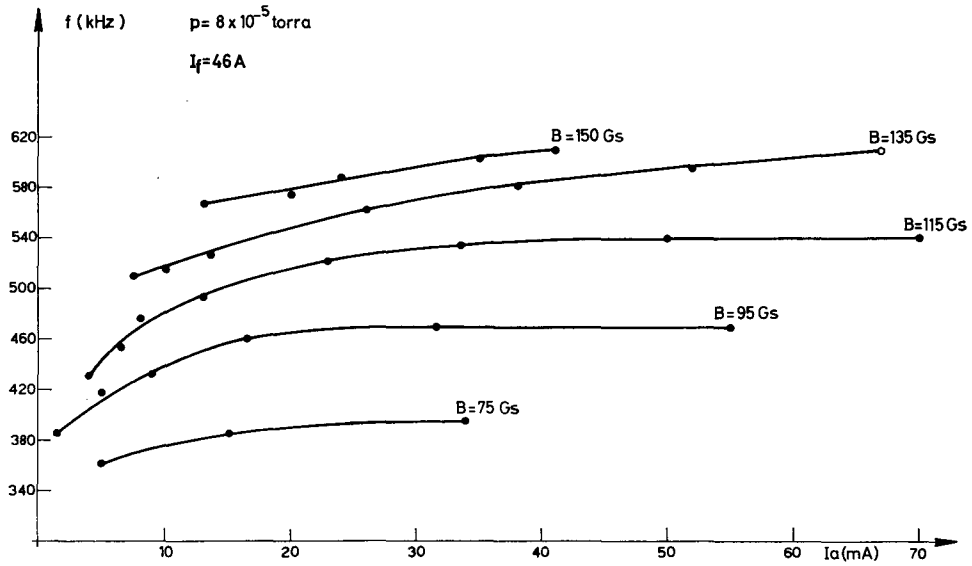

Fig. 18. Frequency of oscillations vs. anode current.

The dependence of the frequency on the magnetic field at different anode currents is shown in Fig. 19. These curves have a linear character with changing slope at about 110 Gs. Increasing pressure leads to decreasing frequency (Fig. 20).

There are different explanations regarding the generation of these oscillations. Experiments of other authors indicate that in cold cathode gas discharge at very low pressure, under the action of crossed-fields, an intense unstable space cloud is formed [**54, 59, 60**]. In the magnetron diode this cloud rotates around the cathode with velocity $v_\theta = E/B$, where E is the radial electric field and B the uniform magnetic field. Since $r\omega = v_\theta$, where ω is the frequency of the electron cloud rotation, we obtain

$$\omega = \frac{E}{rB}, \text{ i.e. } f = \frac{E}{2\pi rB}. \tag{28}$$

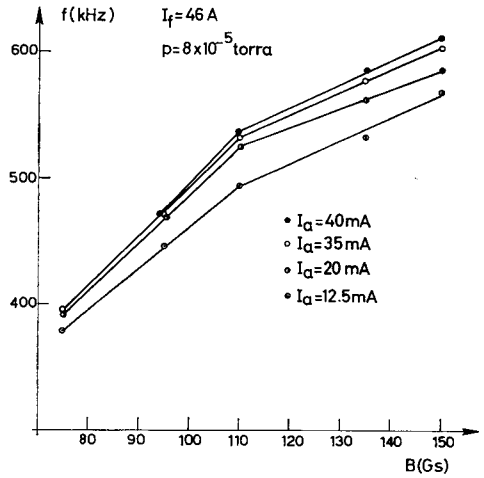

Fig. 19. Frequency of oscillations vs. magnetic field.

If there is a parabolic potential distribution in the magnetron diode, i.e. a linear dependence of E on r, we obtain an isochronal condition, if the rotation frequency does not depend on the radius. Such potential distribution appears in case the space charge is uniform. Therefore, if we assume parabolic potential distribution

$$U(r) = U_a(r/R)^2 \qquad (r_0 \ll R),$$

the electric field becomes

$$E = -2U_a(r/R^2),$$

so that relation (28) can be written in the form

$$f = U_a/(\pi R^2 B). \tag{29}$$

For $U_a = 100$ V, $B = 200$ Gs and $R = 2$ cm, this frequency is about 4 Mc/s.

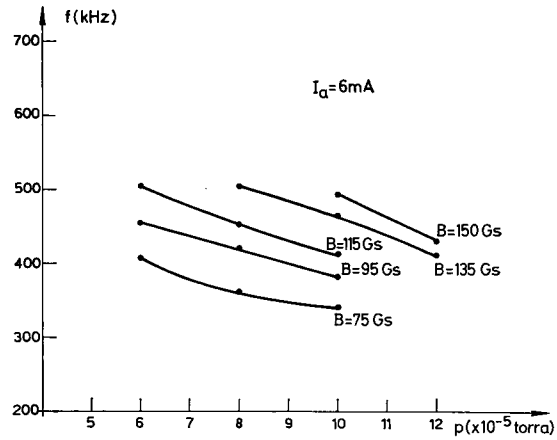

Fig. 20. Frequency of oscillations vs. pressure.

The frequencies measured in our experiments are 10 times lower than theoretical ones. The main discrepancy consists in that the theory predicts decrease in frequency with magnetic field, while experiments obtain increase in frequency. However, the above generation mechanism of these oscillations may be correct because the potential and electric field distribution change when the magnetic field is applied.

One mechanism which can explain these instabilities is related to ion oscillations in the potential well near the cathode. The theory of ion oscillation in a parabolic well gives the frequency

$$f=\frac{1}{2\pi a}\sqrt{\frac{2e}{M}U_m}, \tag{30}$$

where a is the width and U_m the depth of the well, and M ion mass.

If the magnetic field is increased, for example, the electron cloud is confined around the cathode and the potential well becomes deeper and narrower, thus increasing the oscillation frequency. In the case of $U_m = 1$V, $a = 1$ mm, for argon ions we obtain $f = 0.3$ kc/s.

Since the frequency does not change with different gases, it seems that the rotation of the electron cloud can be taken as the generation mechanism of these oscillations.

1.3.2. *Electron transit in the gas magnetron diode at high magnetic fields*

The problem of electron transit in crossed electric and magnetic fields was studied by many authors [**61—67**]. However, electron transit in intense magnetron discharge has not been specially investigated. Since electron transit has an important role in the explanation of the magnetron discharge mechanism, we will devote particular attention to this problem.

Using Eq. (22), which gives the mean drift velocity in radial direction, we can calculate the electron transit time from cathode to anode by

$$T=\frac{R}{v_a}=\frac{8l_s}{\sqrt{\frac{2eU_a}{m}}}\left(\frac{B}{B_c}\right)^3. \tag{31}$$

Introducing $l_s = 4.79 \cdot 10^{-3}$ cm for argon at 1 torr pressure, and numerical values for e and m, we obtain the practical form of Eq. (31)

$$T=6.3\frac{1}{p\sqrt{U_a}}\left(\frac{B}{B_c}\right)^3, \tag{32}$$

where U_a is given in volts, p in 10^{-4} torr and T in μsec. Typical values of T, calculated from Eq. (32), are given in Table II.

TABLE II

Electron transit time in the gas magnetron diode filled with argon ($U_a = 100$ V)

	T(sec)	
p(torr)	$B/B_c = 10$	$B/B_c = 20$
10^{-2}	$6.3 \cdot 10^{-6}$	$5 \cdot 10^{-5}$
10^{-3}	$6.3 \cdot 10^{-5}$	$5 \cdot 10^{-4}$
10^{-4}	$6.3 \cdot 10^{-4}$	$5 \cdot 10^{-3}$
10^{-5}	$6.3 \cdot 10^{-3}$	$5 \cdot 10^{-2}$
10^{-6}	$6.3 \cdot 10^{-2}$	$5 \cdot 10^{-1}$
10^{-7}	$6.3 \cdot 10^{-1}$	5
10^{-8}	6.3	50

The electron transit time was measured experimentally by pulsing the anode voltage. The magnetron diode was submitted to rectangular anode pulses which last 30 μsec with a rise time of 2 μsec (Fig. 21). The wave forms of the anode current and voltage were observed simultaneously (Fig. 22), and the transit time of electrons was determined from the delay of the current pulse.

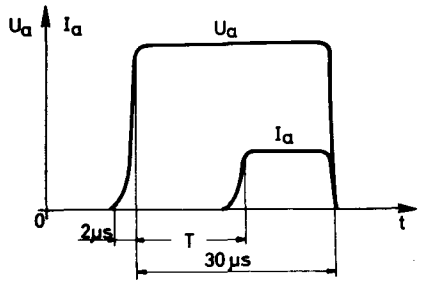

Fig. 21. Assumed waveforms of anode voltage and anode current.

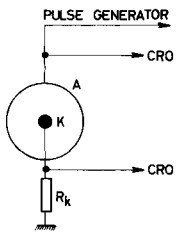

Fig. 22. Circuit for electron transit time measurement.

The working conditions were such that the delay time was in the range 0—30 μsec. Typical oscilloscope traces are shown in Fig. 23. It is seen that the transit time increases with the magnetic field. The experimentally obtained transit time as a function of B is compared with the theoretical curve $T = f(B)$, Fig 24.

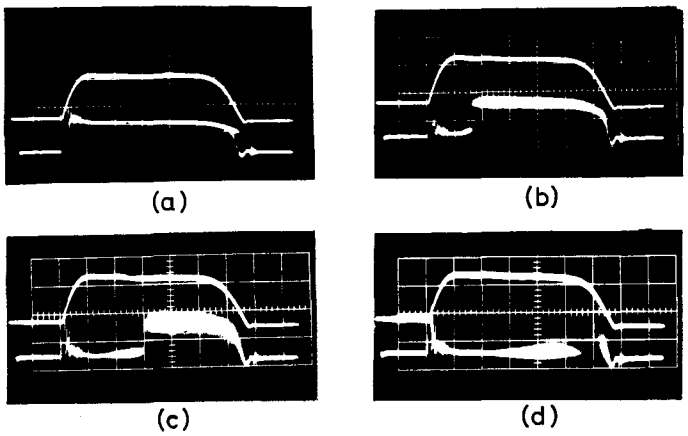

Fig. 23. Typical oscilloscope traces of anode current and anode voltage. $U_a = 320$ V (200V/cm), I_a(20 mA/cm), $p = 10^{-4}$torr, $B_c = 63$ Gs. (a) $B/B_c = 0$; (b) $B/B_c = 2$; (c) $B/B_c = 3{,}2$; (d) $B/B_c = 4{,}8$.

Although in deriving Eq. (32) we used certain approximations and limitations, the experimental results are in good agreement with the theory. The deviations are large at small magnetic fields, because we derived Eq. (32) by assuming a high magnetic field.

It is interesting to obtain a similar expression in another way. Neglecting the gradient pressure term for the time-invariant case, the momentum transfer equation

$$m\frac{dv}{dt} = -\frac{\nabla p}{n} - e(\boldsymbol{E} + \boldsymbol{v} \times \boldsymbol{B}) - m\nu_c \boldsymbol{v} \tag{33}$$

becomes

$$e(\boldsymbol{E} + \boldsymbol{v} \times \boldsymbol{B}) + m\nu_c \boldsymbol{v} = 0, \tag{34}$$

from which we obtain

$$v_d = \frac{\nu_c}{\omega_c}\frac{E}{B}, \quad v_\theta = \frac{E}{B}, \tag{35}$$

where ω_c is the cyclotron frequency ($\omega_c = eB/m$). Since $\nu_c \ll \omega_c$, the mean electron velocity is v_θ, i.e.

$$\nu_c \cong \frac{v}{l_s} = \frac{1}{l_s}\frac{E}{B}. \tag{36}$$

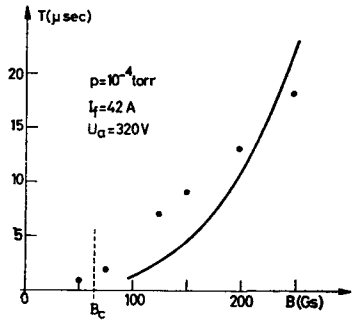

Fig. 24. Electron transit time vs. magnetic field — experimental points and theoretical curve.

Equations (35) and (36) can be combined to yield

$$v_d = \frac{m}{e}\frac{1}{l_s}\frac{E^2}{B^3}. \tag{37}$$

Thus, the expression for electron transit time becomes

$$T = \frac{e l_s}{m} B^3 \int_{r_0}^{R} dr/E^2. \tag{38}$$

Assuming linear potential distribution $U = \frac{r - r_0}{R - r_0} U_a$, we can write T as

$$T = \frac{32 l_s}{\sqrt{\frac{2eU_a}{m}}} \left(\frac{B}{B_c}\right)^3. \tag{39}$$

Therefore, this expression yield a value for the transit time which is four times greater than the result given by Eq. (31). This discrepancy appears because in the earlier case the assumed collisions occur at places of maximum electron energy, but here the collisions occur at mean electron energy, which is twice lower than the maximum energy.

2. PROBLEM OF THE SELF MAGNETIC FIELD

2.1. Introduction

A gas magnetron diode used as an intense ion suorce is characterized by the requirement that electron emission from the cathode should be intense. Besides, since strong cathode sputtering exists, the cathode must be solid. Thus, in the magnetron ion source we use a 1 mm-diameter tungsten filament with 50—60 A supply. This was the reason for the investigation of the influence of the filament heating current upon the diode characteristics without an external magnetic field.

The dependence of the anode current on the filament heating current, for a constant anode voltage, is an important characteristic of the structure. The measurement of this characteristic revealed an interesting effect. Increase in the filament heating current does not lead to saturation of the anode current. The anode current decreases after a critical value (Fig. 25). When the cathode is heated by direct current the anode current drop is more pronounced and the increasing filament current causes the anode current to vanish (Fig. 26).

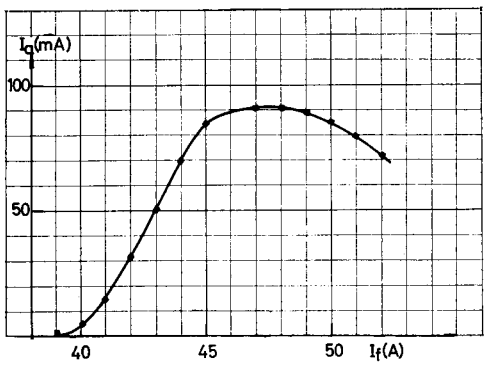

Fig. 25. Anode current vs. cathode heating current (U_a=100 V; alternating heating current).

This phenomenon is ascribed to the influence of the tangential magnetic field B_θ induced by the filament heating current. Namely, due to the influence of B_θ the electron paths are not straight lines since the electrons deflect in the z-direction. Above the critical value of the filament heating current, B_θ is so high that the electrons come back to the cathode and the anode current is cut off (this phenomenon is called self cutoff) (Figs. 27, 28).

2.2. Theoretical and experimental analysis of the self cutoff phenomenon

2.2.1. *Electron motion in the self magnetic field*

Let us consider an electron moving in a radial electric and azimuthal magnetic field. Both fields are inversely proportional to the radial distance r. The electron leaves the cathode at the point $(r_0, 0, 0)$ with initial velocity (u_0, v_0, w_0). Both position and velocity are given in the cylindrical coordinate system co-axial with the diode structure.

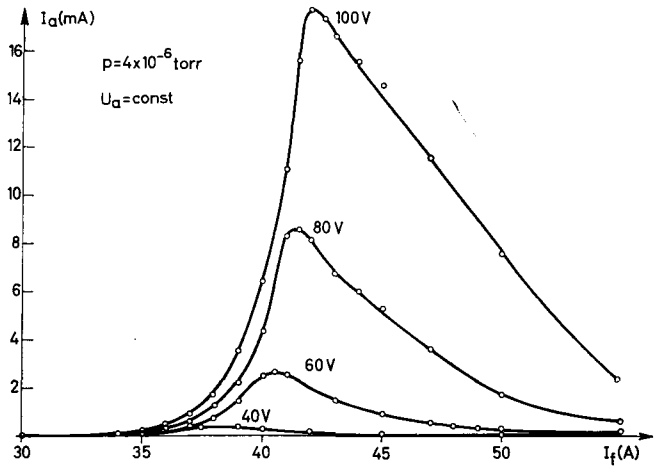

Fig. 26. Anode current vs. cathode heating current (direct heating current).

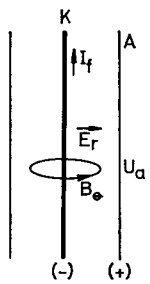

Fig. 27. Geometry of a cylindrical diode with self magnetic field.

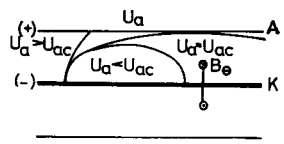

Fig. 28. Electron paths in a cylindrical diode with self magnetic filed.

The equations of motion are:

$$m\left[\frac{d^2r}{dt^2}-r\left(\frac{d\theta}{dt}\right)^2\right]=-eE_r-eB_\theta\frac{dz}{dt}, \tag{40}$$

$$\frac{m}{r}\frac{d}{dt}\left(r^2\frac{d\theta}{dt}\right)=0, \tag{41}$$

$$m\frac{d^2z}{dt^2}=eB_\theta\frac{dr}{dt}, \tag{42}$$

where E_r is the radial electric field and B_θ the Biot-Savart magnetic field of the filament, determined by

$$B_\theta=\mu_0 I_f/(2\pi r). \tag{43}$$

Integration of Eqs. (41) and (42) in relation to time gives

$$r^2\frac{d\theta}{dt}=r_0v_0, \tag{44}$$

(45) $$m\frac{dz}{dt} = ae \ln (r/r_0) + mw_0,$$

where $a = \mu_0 I_f/(2\pi)$.

By introducing $d\theta/dt$ and dz/dt in Eq. (40) we obtain

(46) $$m\frac{d^2r}{dt^2} = mr\left(\frac{r_0 v_0}{r^2}\right)^2 - eE - e\frac{a}{r}\left(e\frac{a}{m}\ln\frac{r}{r_0} + w_0\right).$$

After integration, the last equation can be written in the form

(47) $$\frac{m}{2}\left(\frac{dr}{dt}\right)^2 = \frac{m}{2}u_0^2 + \frac{m}{2}v_0^2\left(1 - \frac{r_0^2}{r^2}\right) + eU_r - eaw_0 \ln (r/r_0) - \frac{e^2a^2}{2m}\ln^2 (r/r_0),$$

where U_r is the potential of the point at radial distance r. The radial distance of the electron is maximum when its radial velocity is zero. Assuming that this occurs at the critical anode voltage $U_a = U_{ac}$, from Eq. (47) we obtain

(48) $$U_{ac} = aw_0 \ln (R/r_0) + \frac{ea^2}{2m}\ln^2 (R/r_0) - \frac{2e}{m}v_0^2\left(1 - \frac{r_0^2}{R^2}\right).$$

If the anode voltage is lower than U_{ac} the anode current is cut off (hence we termed the phenomenon *self-cutoff*).

Equation (48), which gives the self-cutoff condition, may be greatly simplified if the electron initial velocity can be neglected. In this case, taking into account the value for a, we obtain

(49) $$U_{ac} = \left[\frac{e\mu_0^2}{8m\pi^2}\ln^2 (R/r_0)\right] I_f^2.$$

Since the expression in the brackets only depends on geometric factors, Eq. (49) can be written in the form

(50) $$U_{ac} = \alpha I_f^2.$$

Introducing the numerical values for e, m, μ_0 we obtain the practical form of Eq. (49)

(51) $$U_{ac} = 0{,}00352 \ln^2 (R/r_0)\, I_f^2,$$

where U_{ac} is given in volts and I_f in amperes.

From the above analysis it is clearly seen that the anode current can be cut off by the action of the self magnetic field, i.e. the diode placed in the working regime characteristic for a magnetron diode. Thus, we have a new type of magnetron, which is similar to plane magnetron, because of its characteristic electron path. On the other hand, Eq. (50) has a form analogous to Hull's relation (9).

As the diode length is finite, it is of iterest to evaluate the range of the electron in the z-direction for the critical case, when the trajectory glances the anode ($U_a = U_{ac}$). Neglecting initial velocity, the Eqs. (45) and (47) take the form

(52) $$m\frac{dz}{dt} = ae \ln r/r_0,$$

(53) $$\frac{m}{2}\left(\frac{dr}{dt}\right)^2 = eU_r - \frac{e^2a^2}{2m}\ln^2\frac{r}{r_0},$$

from which we get

$$\frac{dr}{dz}=\left[\frac{2m}{a^2e}\frac{U_r}{\ln^2 r/r_0}-1\right]^{1/2}. \tag{54}$$

Note that the self- cutoff condition (49) is independent of the potential distribution. However, the form of the electron trajectory depends on the potential distribution. Neglecting the space charge we have

$$U_r=U_a\frac{\ln r/r_0}{\ln R/r_0}.$$

If we introduce the condition (49) in Eq. (54) combining with the logarithmic potential distribution, the equation of the trajectory of the electron moving under the action of E_r and B_θ becomes

$$\frac{dr}{dz}=\left[\frac{\ln R/r_0}{\ln r/r_0}-1\right]^{1/2}, \tag{55}$$

so that the range of the electron in the z-direction is

$$z_0=\int_{r_0}^{R}\frac{dr}{\left[\frac{\ln R/r_0}{\ln r/r_0}-1\right]^{1/2}}. \tag{56}$$

Introducing the new variable s into Eq. (56) by

$$\frac{\ln r/r_0}{\ln R/r_0}=1-s^2,$$

we obtain

$$z_0=2r_0\ln(R/r_0)\int_0^1(1-s^2)^{1/2}(R/r_0)^{1-s^2}\,ds. \tag{57}$$

Taking, for example, $r_0=0.5$ mm, $R=17.5$ mm, numerical integration yields $z_0=5.4$ cm, which indicates that the end effects are important, because z_0 is of the order of the diode length. As an experimental proof we can use the dependence of anode current on filament heating current, when the anode current slowly decreases with I_f, which is not the case with the diode with an axial magnetic field.

2.2.2. *Electron motion under the action of self magnetic and axial magnetic fields*

The equations of electron motion under the action of the filament magnetic field B_θ, external magnetic field B and radial electric field E_r are

$$m\left[\frac{d^2r}{dt^2}-r\left(\frac{d\theta}{dt}\right)^2\right]=-eE_r-er\frac{d\theta}{dt}B-e\frac{dz}{dt}B_\theta,$$

$$m\left[\frac{1}{r}\frac{d}{dt}\left(r^2\frac{d\theta}{dt}\right)\right]=e\frac{dr}{dt}B,$$

$$m\frac{d^2z}{dt^2}=e\frac{dr}{dt}B_\theta.$$

This system can be integrated in the same way as if we have either B or B_0 only. Neglecting the initial velocity, the critical anode voltage can be presented by the following relation:

$$U_{ac}=\left[\frac{e\mu_0^2}{8m\pi^2}\ln^2\frac{R}{r_0}\right]I_f^2+\left[\frac{e}{8m}R^2\left(1-\frac{r_0^2}{R^2}\right)^2\right]B^2, \tag{58}$$

i.e.

$$U_{ac}=\alpha I_f^2+\beta B^2. \tag{59}$$

Thus, the critical anode voltage is the sum of the critical anode voltage for the cutoff in the external and filament magnetic fields when applied separately. Equation (58) permits the correction of the cutoff criterion in an external magnetic field when the filament heating current is considerable.

2.2.3. *Experimental proof of the self-cutoff phenomenon*

When the cathode is heated by alternating current, the anode current cutoff appears during the time interval p in which the heating current is higher than critical (Fig. 29). This interval increases if the heating current increases or if the anode voltage decreases.

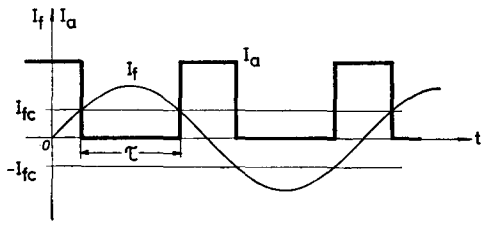

Fig. 29. Theoretically obtained waveform of anode current.

The experimentally obtained waveforms of the anode current together with the filament current waveforms (50c/s) are shown in Fig. 30. The measurement was made with a constant filament current (50 A), for the following values of the anode voltages: (a) 40 V, (b) 60 V, (c) 100 V, (d) 150 V, (e) 180 V, (f) 220 V. The waveforms

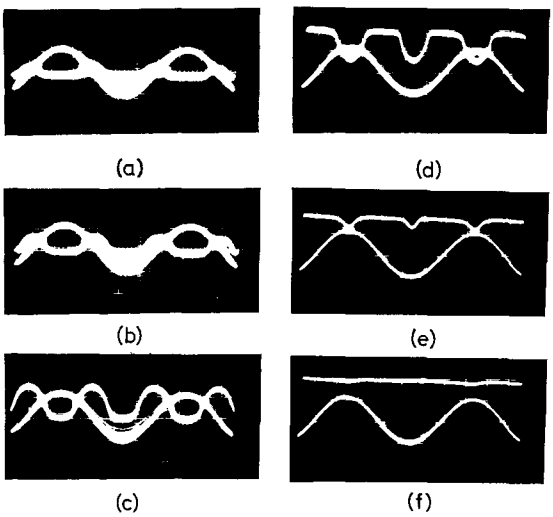

Fig. 30. Experimentally obtained waveforms of anode current.

(a), (b), (c) clearly show total cutoff during the time interval τ. The anode current only flows when the filament current is below the critical value. Further increase in the anode voltage diminishes the influence of the filament magnetic field ((d) and (e)). The waveform (f) illustrates the condition in which sufficiently high anode voltage is applied, so that the peak value of the filament current is less than critical and the influence of the self magnetic field is negligible.

2.3. **Dependence of self-cutoff conditions on diode dimensions**

From Eq. (53) it can be concluded that the critical anode voltage depends on the heating current and diode dimensions. On the other hand, since the heating current is a function of the cathode cross-section, the self-cutoff condition only depends on diode dimensions (R, r_0). Assuming constant cathode temperature, we can write [75]

$$I_f/d^{3/2} = k\,, \tag{60}$$

where $k = f(T)$ (I_f is given in amperes, $d = 2r_0$ in centimeters), so that Eq. (53) becomes

$$U_{ac} = 0.02816\, k_2 r_0^3 \ln^2 R/r_0\,. \tag{61}$$

Equation (61) shows that U_{ac} is rapidly increasing function of r_0 for small values of r_0. However, since $\ln R/r_0$ is a decreasing function of r_0 and it reduces to zero at $R = r_0$, it follows that U_{ac} reaches the maximum value. From the condition $dU_{ac}/dr_0 = 0$ follows $r_0/R = 1/e^{2/3}$, where e is the base of natural logarithm, so that

$$U_{ac} = 0{,}0017\, k^2 R^3. \tag{62}$$

For example, if $T = 2500$°K and $R = 17{,}5$ mm, we have $U_{ac\,\max} = 21000$ V, while the filament heating current is 1500 A. Naturally, such working conditions have no practical significance, because we only observed the case of the small cathode diameter.

Figure 31. is a plot of the function given by Eq. (61), for different cathode temperatures, evaluated for $R = 17.5$ mm.

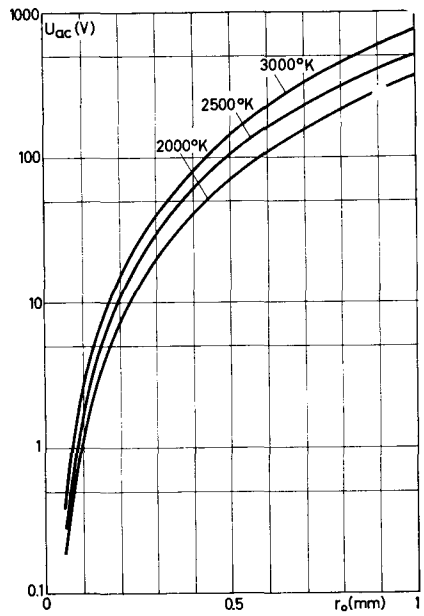

Fig. 31. Critical anode voltage as a function of cathode radius for different cathode temperatures.

2.4. **Influence of the self magnetic field on the broadening of the cutoff magnetron characteristic**

In many experiments it was observed that the fundamental magnetron characteristic $I_a = f(B)$ did not have as sharp a drop near the cutoff as predicted by Hull's theory [68—73]. The effects which can cause this phenomenon are:

— existence of an energy distribution of the emitted electrons,

— inhomogeneity of the axial magnetic field,

— magnetic field is not collinear with diode axis,
— mechanical distortion of the filament,
— presence of the residual gas,
— finite diode length — end effects,
— appearance of fast electrons,
— influence of the axial electric field, due to filament heating current,
— influence of the self magnetic field, induced by alternating filament heating current.

The importance of particular effects is connected with the diode dimensions and working conditions. In case the magnetron diode is an intense ion source, the influence of the filament heating current is largest.

If the cathode is heated by alternating current, the critical anode voltage changes as

$$U_{ac} = \alpha I_{f\max}^2 \sin^2 \omega t + \beta B^2, \tag{63}$$

whence we obtain

$$\beta B^2 \leqslant U_{ac} \leqslant \alpha I_{f\max}^2 + \beta B^2.$$

Thus, if $U_a < \beta B^2$, the anode current is permanently cut off; if $\beta B^2 < U_a < \alpha I_{f\max}^2 + \beta B^2$, the cutoff only appears in a certain time interval; if $U_a > \alpha I_{f\max}^2 + \beta B^2$, the anode current is not cut off.

After assuming that the anode current varies with anode voltage as (Fig. 32)

$$I_a = \begin{cases} I_0 & U_a > U_{ac} \quad (0 < t < t_1;\ t_0 - t_1 < t < t_0) \\ 0 & U_a \leqslant U_{ac} \quad (t_1 < t < t_0 - t_1, \end{cases} \tag{64}$$

the average value of anode current becomes

$$I_a = 2 \frac{t_1}{t_0} I_0 \quad (0 \leqslant t_1 \leqslant t_0/2). \tag{65}$$

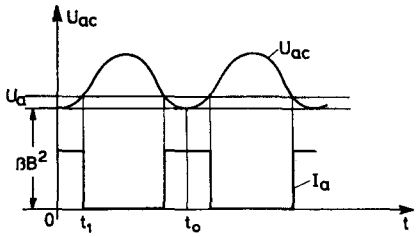

Fig. 32. Theoretically obtained waveform of anode current for a diode with dc axial and ac self magnetic fields.

Thus, calculating t_1, we obtain a relation between I_a and B. For a given U_a the time t_1 can be calculated from

$$U_a = \alpha I_{f\max}^2 \sin^2 \omega t + \beta B^2,$$

so that

$$t_1 = \frac{1}{\omega} \arcsin \sqrt{\frac{U_a - \beta B^2}{\alpha I_{f\max}^2}}.$$

Since $t_0 = \pi/\omega$, Eq. (65) becomes

$$\frac{I_a}{I_0} = \begin{cases} \dfrac{2}{\pi} \arcsin \sqrt{\dfrac{U_a - \beta B^2}{\alpha I_{f\max}^2}} & (U_a - \beta B^2 \leqslant \alpha I_{f\max}^2), \\ 1 & (U_a - \beta B^2 \geqslant \alpha I_{f\max}^2). \end{cases} \tag{66}$$

In case $r_0 = 1$ mm, $R = 17.5$ mm, $I_f = 50$ A, when $\alpha I_{f\max}^2 = 220$, $\beta = 0.064$ (U_a is given in volts, B in gauss), the function (66) is presented in Fig. 33. The three curves are plotted for anode voltages of 200, 220 and 250 V. Namely, for $U_a = 200$ V the anode current cutoff appears even though no external magnetic field is applied, while for $U_a = 250$ V the self cutoff at $B = 0$ does not exist. For $U_a = 220$ V we have the critical case when $U_a = \alpha I_{f\max}^2 = U_{ac}$.

The analysis described above indicates a change of U_{ac} due to the existence of the alternating self magnetic field. If we have dc filament heating, the cutoff appears at a magnetic field lower than B_c, and the characteristic $I_a = f(B)$ descreases sharply near the cutoff.

The experimental curves are given in Fig. 34. The first one is related to the case $2r_0 = 0.5$ mm and the second $2r_0 = 1$ mm. From these curves we can clearly see the broadening of the characteristic $I_a = f(B)$ at higher filament heating currents, so that ac filament heating introduces a systematic error in the measuremet of the cutoff characteristic

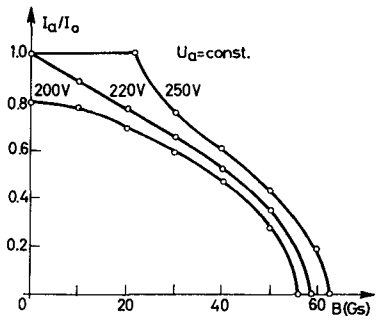

Fig. 33. Anode current vs. axial magnetic field at ac cathode heating current (theoretical curve).

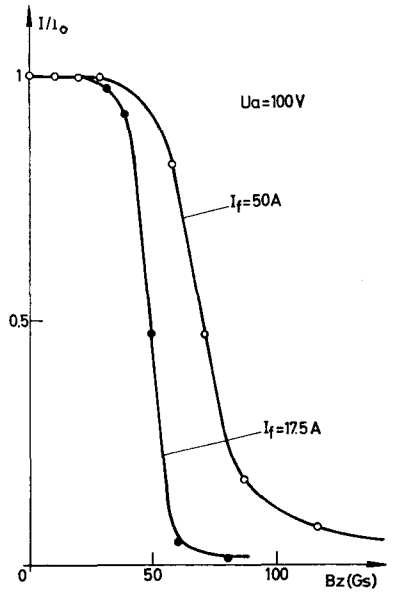

Fig. 34. Anode current vs. axial magnetic field at ac cathode heating current (experimental curves).

widts. Thus, in such measurements we must take into account the influence of I_f, in spite of the small cathode diameter.

2.5. **Gas discharge under the influence of the self magnetic field**

A cylindrical diode with axial magnetic field and radial electric field represents the system with crossed-fields. However, in case $B = 0$ we also have the crossed-fields system, because B_θ exists, which implies that the characteristics of such geometry could be similar to the characteristics of the gas magnetron diode.

For illustration, waveforms of the anode current together with sinusoidal filament heating current were studied. The waveform of the anode current at high pressure is given in Fig. 35. A gas discharge starts at small B_θ, and at a certain critical value of B_θ there is a sharp cutoff. At lower pressures and higher I_f the influence of B_θ on the anode current is greater. The waveform of the anode voltage is a double square pulse (Fig. 36). The central part of the pulse corresponds to weak B_θ, when gas discharge is not initiated. The amplified parts of the pulse for higher B_θ exist because gas discharge is initiated. It can be noticed that the time duration of these parts is not equal. The narrower part corresponds to decreasing B_θ and the wider to increasing B_θ, which is quite analogous to the hysteresis characteristic of the gas magnetron diode.

As the best illustration of the role of B_θ in initiating gas discharge, we can use the waveform of the anode current shown in Fig. 37, where the anode current waveform is followed by the noise, characteristic of every discharge.

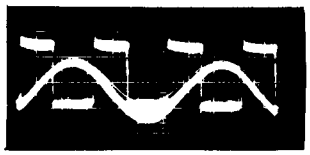

Fig. 35. Waveforms of anode current and cathode heating current ($p = 10^{-4}$ torr, $U_a = 50$ V, $U_a = 50$ V, $I_f = 45$ A).

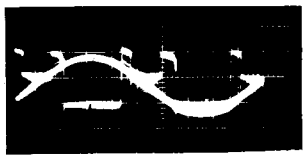

Fig. 36. Waveforms of anode current and cathode heating current ($p = 2 \cdot 10^{-4}$ torr, $U_a = 60$ V, $I_f = 50$ A).

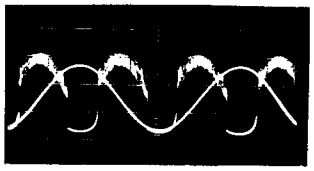

Fig. 37. Waveform of anode current with characteristic noise.

The dependence of the anode current on dc filament heating current, for different anode voltages, is shown in Fig. 38. In this case we can also achieve a sharp cutoff, as in the case of the gas magnetron diode.

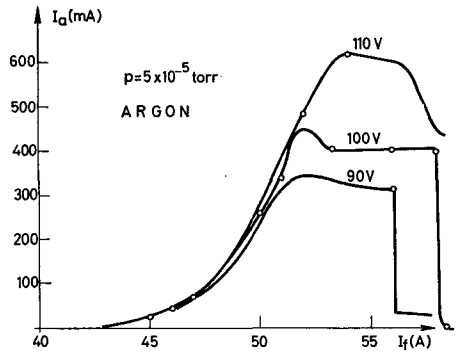

Fig. 38. Anode current vs. cathode heating current (gas diode).

3. APPLICATIONS OF THE GAS MAGNETRON DIODE

The first theory of the magnetron diode was developed in 1921 by A.W. HULL, and every since then much time has passed before the first technical application of such configuration. Namely, the first resonant magnetron appeared before Vorld War II and mass production began during the war.

However, magnetron geometry is not only convenient for the excitation and maintenance of high frequency oscillations. Its application is diverse because of the many phenomena related to the influence of the magnetic field on the gas magnetron diode. The most important application is related to ion sources, which in fact represent the gas magnetron diodes with ion extraction. On the other hand, the magnetron diode may be used as ionization gauges for vacuum measurement. Such tubes can be used as ion pumps for obtaining extremely high vacuum, because of their high degree of ionization. The cold cathode magnetron diode under certain conditions can operate as a voltage filter with a variable pass-band [**45**]. Presently there is no hope for the gas magnetron diode to be used as a noise generator or a low frequency oscillator, for classical means can hardly be surpassed. However, the application of the gas magnetron diode as a high power oscillator, using the switching action of the magnetic field, deserves consideration.

3.1. **Gas magnetron diode as an intense ion source**

The first use of an ion source with magnetron geometry dates from 1934 [**26**]. In order to obtain intense ion beams with this source some attempts were made in 1938 [**27—29**]. However, since then for two decades, nothing was done to improve the magnetron source.

The development of the magnetron ion source started in our Laboratory in 1957 [**30**]. The first ion source was built for the sector-type electromagnetic isotope separator [**74**].

3.1.1. *The principle of obtaining an intense ion beam*

The magnetron ion source is in fact a magnetron diode with the possibility of ion extraction. A schematic diagram of the ion source with applied electric and magnetic fields is given in Fig. 39. Under combined action of forces created by these fields, the electrons move along spiralized paths, which are much longer than the distance between the cathode and the anode. Since the number of ions formed by one electron is proportional to the electron path length, an enhanced ionization can be expected in this source. Two isolated metallic reflector discs placed at the

ends of the source chamber are usually at the cathode potential, so that near these electrodes there is an axial retarding electric field, which reflects the electrons toward the center.

The electron-neutral collisions lead to gas ionization. Under the action of weak magnetic fields direct ionization occurs because the electrons obtain high energy, but at intense magnetic fields the electron energy is lower than the ionization energy. Thus, in this case ionization is possible either by succesive collisions or collisions by fast electrons. Ion concentration is proportional to electron density and since electron density increases with magnetic field in such condition we obtain intense ion beam. Certainly, at a very high magnetic field, electron energy decreases resulting in decreased extracted ion beam intensity and increased recombination processes. On the other hand, the magnetic field influences the conditions of ion extraction, i.e. at intense magnetic field high electron density shields the electric field of the extraction electrode, so that in spite of high ion density, we extract a weak ion beam.

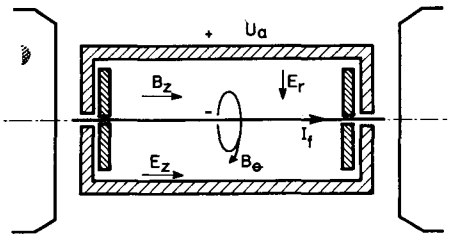

Fig. 39. Schematic diagram of the magnetron ion source.

3.1.2. *Description of the magnetron ion source and method of obtaining an intense ion beam*

The cylindrical anode, made of graphite of stainless steel, is 35 mm in diameter and 72 mm long. The diameter of the tungsten filament is 1 mm. Two isolated graphite or metallic reflector discs are placed at each end of the filament. Gas is let in the source chamber through a needle valve. The isolated metallic sputtering probe, polarized negatively in respect to the anode, is fixed to the bottom of the source chamber (Fig. 40). The source is placed between the poles of an electromagnet with a magnetic field up to 700 Gs. The filament is heated with a current of the order of 50 A. The anode is at 400 V positive potential in respect to the cathode. At a gas pressure of 10^{-3} torr the discharge current is up to 4 A. The ion beam extracted radially by Pierce's electrode system. A photograph of the magnetron ion source is given in Fig. 41. When gas discharge in the source is initiated, the supporting gas ions are accelerated toward the sputtering probe bombarding it intensely.

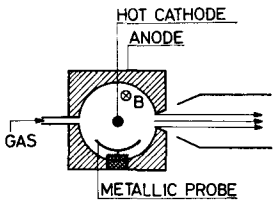

Fig. 40. Magnetron ion source with sputtering probe.

The supporting gases were N_2, A, Kr, Xe, while the sputtering probes were foils of Cu, Ag, Ni, Fe, Ti, Mo, W, Ir, etc. The typical working conditions were: U_a= 100—200 V, I_a= 2—4 A, B=200—400 Gs, the sputtering probe current 0.5 A at a negative potential of 800 V.

Analysis of the ion beam composition indicates a considerable percentage of multi-charged ions: 15% of X^{2+} and 2% of X^{3+} with respect to X^+. The ion beam current of gas elements on the collector of isotope separtor was up to 5 mA, and for metal elements it was about 10 times smaller.

The sputtering probe considerably disturbs the magnetron geometry. The specific configuration of the magnetron diode enables the development of a new method of producing ion beams of high melting point materials. Instead of the application of the sputtering probe, the material was directly fixed to the cathode. Namely, when gas discharge in the source is established, the supporting gas ions bombard and sputter the cathode intensely. The sputtered material is introduced into the discharge, so that we obtain an intense ion beam of high melting point elements.

This way of producing metallic vapours has several advantages with respect to other methods. The fixed material is heated to 2000°C, the density of ions which bombard the cathode is maximum near the cathode, the sputtered particles are introduced into the region of maximum ionization, while the dissipated energy is considerably smaller and the magnetron geometry is not distrurbed.

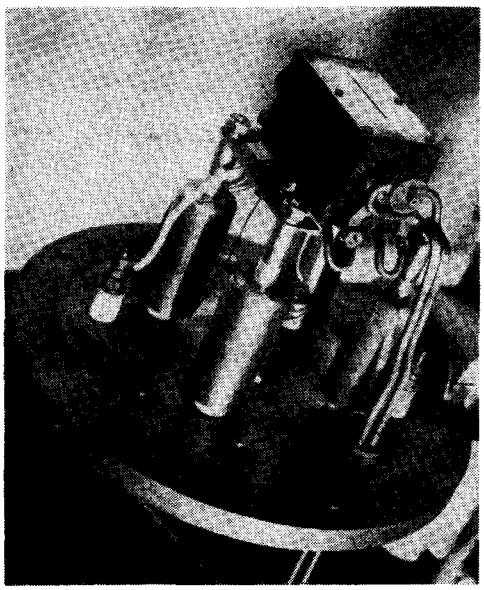

Fig. 41. Magnetron ion source.

The following procedure was developed: the middle of the cold tungsten filament was coated with an emulsion of powdered material, amylacetate and collodium, while the filament ends were left uncovered (Fig. 42). The filament was gradually heated to red hot at atmospheric pressure. After cooling, the filament was coated with a new layer of emulsion and the heating was repeated. This procedure was performed several times

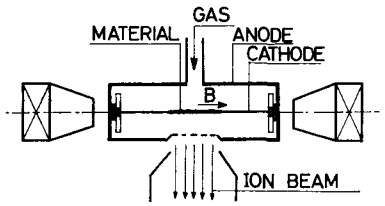

Fig. 42. A new method of producing ion beams.

until desired thickness was obtained. In this way it was possible to fix to the cathode a quantity of about 100 mg of material. Only the filament ends emit primary electrons, because the central part is at a lower temperature. However, under the action of ion bombardment this part of filament emits secondary electrons. This method was checked on Ir, Ni, Ce, Ce_2O_3, La, Nd_2O_3, whose melting points are up to 3000°C. The intensities of the ion beams on the separator collector are given in Table III.

TABLE III

Element	Ir	Ni	Ce	La	Nd
Current (μA)	50	100	70	200	70

In addition, we should say that the extracted ion beams is much more intense than the collected beam, since the lenghts of the separator tube is about 3 meters.

It was interesting to investigate the influence of the magnetic field on the intensity of the collector current I_c. The dependence $I_c = f(B)$ together with $I_a = f(B)$ is given in Fig. 43. As can be seen, I_c is proportional to I_a, so that in cutoff conditions the intensity of ion beam is negligible. In the presence of a high magnetic field an intense but weakly focused ion beam is extracted, which indicates that ion beam has wide energy spread.

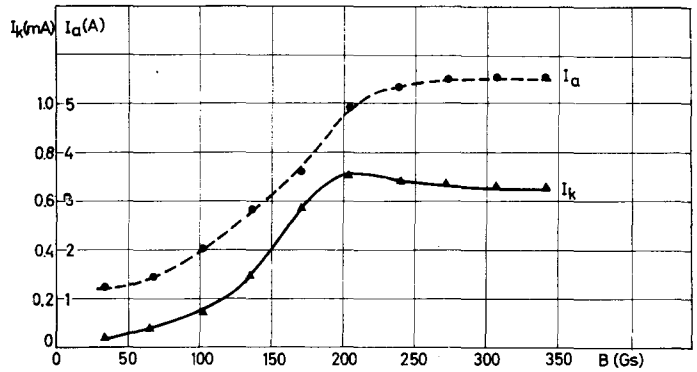

Fig. 43. Anode current and collector ion current vs. axial magnetic field ($U_a = 100$ V).

In the magnetron ion source the cathode is submitted to intense ion bombardment which leads to cathode destruction. Since the ions give their kinetic energy to the cathode, we can decrease the filament heating current. At a certain critical value of the anode current we can completely switch off the heating current, so that a self sustained gas discharge occurs. Thus, the cathode life time is increased by about two times. Since the gas discharge is most intense in the central part of the diode, the cathode breaks in the middle constantly reducing in size while the magnetron gas discharge transforms to Penning discharge.

3.1.3. *Analysis of the ion beam composition extracted from the magnetron ion source*

The most important characteristic of the magnetron ion source is that it is relatively simple to obtain a wide scale of elements and large amounts of multi-charged ions. In this paragraph we will present a method for the analysis of the ion beam composition, particularly the influence of ion source parameters on the quantity of multi-charged ions.

The ion beam composition was investigated by the standard mass spectrometric method on the electromagnetic isotope separator (sector type magnet $\varphi = 60°$, $r = 75$ cm, $B_{max} = 10$ kGs, maximum acceleration voltage 60 kV). The schematic diagram of the experimental arrangement is given in Fig. 44. The length of the ion path from the source to the analyzing magnet was 130 cm and the whole path from the source to the collector was 340 cm. The residual pressure was at least $7 \cdot 10^{-6}$ torr and was regulated by direct gas inlet into the analyzing chamber.

Due to the long ion path and presence of the residual gas, the ion motion through the analyzing tube is followed by processes which arise in ion-neutral inelastic collisions. Since the ion composition changes, we must take these processes into account.

The identification of apparent masses is based on the following analysis. The kinetic energy of the extracted ions is given by

$$\frac{1}{2} m_1 v^2 = k_1 eU , \tag{67}$$

where k_1 is degree of ionization. If the ion suffers an inelastic collision with a slow neutral, in which m_1 changes to m_2 and k_1 to k_2, then ion motion through the magnetic analyzer is described by the relation

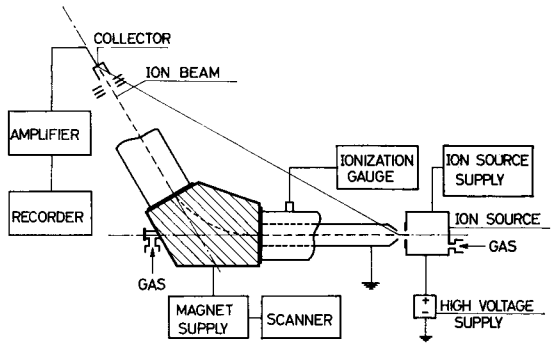

Fig. 44. Schematic diagram of the experimental arrangement.

$$m_2 v/R = k_2 eB , \tag{68}$$

where R is the ion path radius in the magnet. By eliminating v from Eqs. (67) and (68) we obtain

$$R = \frac{1}{B} \sqrt{2 \left(\frac{m_2^2}{m_1} \frac{k_1}{k_2^2} \right) \frac{U}{e}} , \tag{69}$$

so that the extracted ion will be analyzed as an ion with apparent mass

$$m_p = \frac{m_2^2}{m_1} \frac{k_1}{k_2^2} . \tag{70}$$

In case there is no change in ion mass ($m_1 = m_2 = m$), we have

$$m_p = m \frac{k_1}{k_2^2} . \tag{71}$$

For the investigated ion energies and residual gas pressures the following inelastic processes with charge-exchange are observed:

$$X^{2+} \rightarrow X^+, \quad X^{3+} \rightarrow X^{2+}, \quad X^{2+} \rightarrow X^+, \quad X^+ \rightarrow X^{2+} .$$

For example, the apparent masses of argon ions appear to be 120, 30, 80, 10 respectively.

The composition of argon mass spectrum is measured as a function of the anode voltage, magnetic field and gas pressure, when gas discharge current is 3 A. The composition of the argon beam as a function of U_a and p is given in Tables IV and V. The ion currents are obtained by summing the currents from the processes described above. The gas pressure is measured in the analyzing chamber, and estimated in the ion cource (about 100 times higher than in the chamber).

As can be seen, with increasing anode voltage the yield of A^{2+} and A^{3+} increases. This yield slightly changes with pressure, but at higher pressures the recombination processes increase, so we do not know the exact ion beam composition since the yield of fast neutrals was not measured.

TABLE IV

Dependence of argon ion spectrum on anode voltage (I_a=3A, B=100 Gs, U_{ext}=30 kV)

	A^+	A^{2+}	A^{3+}
U_a(V)		Intensity %	
100	96.61	3.27	0.12
125	92.59	6.99	0.42
150	92.38	7.20	0.42
175	89.02	10.45	0.53
200	87.63	11.79	0.58

TABLE V

Dependence of argon ion spectrum on pressure (I_a=3A, U_a= 150 V, B=150 Gs, U_{ext}=40 kV)

	A^+	A^{2+}	A^{3+}
$p(10^{-6}$ torr)		Intensity %	
8.2	90.53	8.76	0.71
8.8	90.63	8.70	0.67
9.4	90.66	8.73	0.61
11	89.55	9.85	0.60
13	89.25	10.19	0.56
15	86.72	12.68	0.60
17	85.41	13.84	0.75
19	83.80	15.44	0.76
24	80.82	18.41	0.77
30	77.05	22.24	0.71

The yield of multi-charged ions rapidly increases with magnetic field up to B_c (cutoff), but at higher magnetic fields this yield remains constant, which is in good agreement with spectroscopic measurements, where intensities of ion spectral lines do not change at over-critical magnetic fields. For magnetic fields lower than B_c the process of direct ionization is the most probable one. With increasing B from zero to B_c the electron path length increases monotonically, while the electron energy remains constant. Thus, the yield of multi-charged ions increases. On the other hand, at higher magnetic fields the number of virtual cathodes increases, but the electron energy decreases, so that we can expect a constant yield of multi-charged ions.

The ion spectrum composition from the magnetron ion source of several elements is given in Table VI.

TABLE VI

Element		Intensity %	
	X^+	X^{2+}	X^{3+}
A	83.10	16.41	0.49
Ti	89.90	10.10	/
Mo	72.90	23.90	3.26
Ag	96.80	3.20	/
Sb	87.00	13.00	/
W	77.90	18.88	3.22

3.1.4. *Conclusion*

The results presented above indicate that the magnetron ion source has remarkable advantages over other ion sources:

a) the construction of the source is very simple;

b) the yield of multi-charged ions is considerable;

c) the source is applicable to a large scale of elements, particularly to high melting point elements;

d) the total source power is not higher than that of conventional sources for low melting point materials, so that there is no need for special materials for source construction.

3.2. **Magnetron ion source for a mass spectrometer**

Using the essential design characteristics of the previously described intense ion source, a miniature mass spectrometer ion source was developed. The schematic diagram of this source is given in Fig. 45. As can be seen, the geometry is quite similar to that of an intense ion source, with some differences in the extraction system.

The material to be analyzed is fixed to the cathode by the same procedure described above. The ion source is made of stainless steel. The anode is 26 mm long and 6 mm in diameter. The tungsten cathode, 0.25 mm in diameter, is heated by 5 A. The anode voltage was in the range 120—200 V and the anode current up to 10 mA. The maximum axial magnetic field was about 300 Gs. The source is investigated in the sector field mass spectrometer (R = 30 cm, φ=60°, U_{ext}=5 kV).

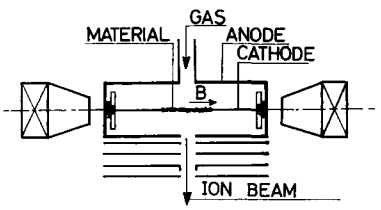

Fig. 45. Schematic view of a miniature magnetron ion source.

The source is mainly used with high melting point materials and their oxides. The list of investigated elements, together with the melting points and corresponding collector currents, is given in Table VII.

TABLE VII

Element or compound	Melting point (°C)	Collector current (10^{-12}A)
Sb	630	50
La	826	80
Nd_2O_3	840	7
Cu	1080	30
Ni	1452	50
Ce_2O_3	1692	10
Ti	1800	4
Ir	2440	2
ZrO_2	2700	5
Ta	2996	3
Re	3167	2

The results show that ion currents are almost independent of the melting temperature. The quantity of the powdered material was 0.5—2 mg, while the ion current was stable 20—60 minutes.

The energy spread of the source was measured by the retarding potential method and the ion beam deflection method (Figs. 46 and 47). The obtained results were compared with Nier's ion source and measurements were carried out in argon, because the ion beam of high melting point materials cannot be obtained in Nier's ion source. The measurements indicate that the differences in the distribution curves in both cases are negligible, so that the magnetron ion source can be successfully applied for analytical purposes.

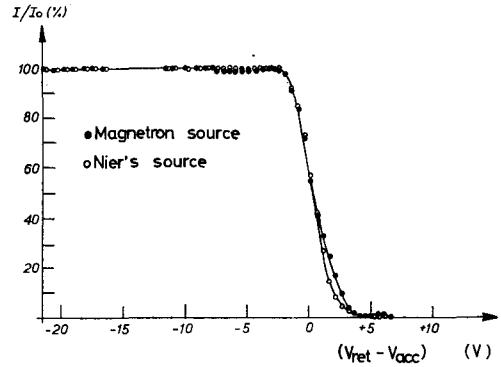

Fig. 46. Relative extracted ion current vs. difference of retarding and accelerating voltages.

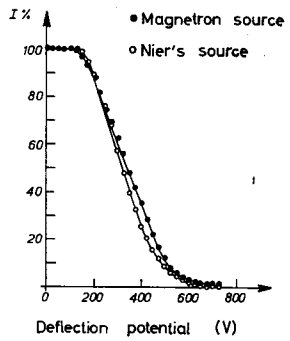

Fig. 47. Relative extracted ion current vs. diflection potential.

3.3. A new modification of the magnetron ionization gauge

Magnetron gas discharge is known to be very suitable for increasing the sensitivity of vacuum ionization gauges. Several papers [**19—22**] describe ionization gauges with magnetron geometry, in which the sensitivity coefficient is increased by a few orders of magnitude as compared with standard ionization gauges. Besides, the magnetron diode offers exceptional properties for pressure measurement in ultra high vacuum, up to 10^{-14} torr, since the effect of X-radiation is avoided when the magnetic field is much higher than critical. Our aim was to develop a highly sensitive magnetron gauge of simple geometry and construction. For this purpose we used split-magnetron configuration.

3.3.1. *Split-magnetron ionization gauge*

A schematic view of the split-magnetron gauge is given in Fig. 48. The electrode system consists of an axial hot cathode and anode cylinder split up into two symmetrical parts. One half of the cylinder is used as the anode and the other as ion collector. The electrode system is enclosed in a glass envelope. The ionization gauge is placed in the axial magnetic field. The cathode is a tungsten filament 0.15 mm in diameter and 60 mm long. The anode-ion collector is 24 mm in diameter, 60 mm long. The slit between the anode and the ion collector is 3 mm. The working parameters are: filament heating current 1.1—1.4 A; electron emission current 0—10 mA; anode voltage 0—500 V; ion collector voltage —20 V; magnetic field 0—400 Gs.

3.3.2. *Experimental results*

The split-magnetron ionization gauge was investigated by comparing it with a standard ionization gauge in a common glass vacuum system. Figure 49 shows the dependence of the ion collector current on the electron emission current. It can be seen that there is a linear dependence between the number of produced and collected ions and the number of primary electrons within a wide range.

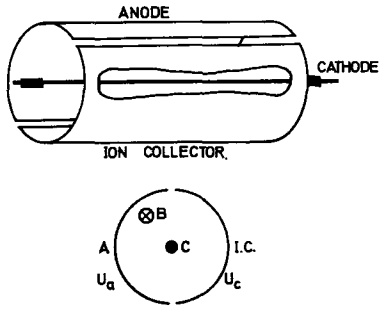

Fig. 48. Split-magnetron ionization gauge.

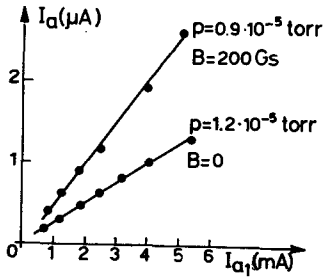

Fig. 49. Collector current vs. emission current.

Thus, the relation for standard ionization gauges

$$I_c = kI_e p,$$

where I_c is the ion collector current, k sensitivity coefficient, I electron emission current and p pressure, is also valid in the case of a split-magnetron gauge. On the other hand, the sensitivity coefficient increases with the magnetic field. For example, at $B=0$ we have $k=20$, and at $B=150$ Gs $k=52$, while the sensitivity coefficient of standard ionization tubes is in the range 10—20.

The dependence of ion collector current on gas pressure, without and with magnetic field, is shown in Fig. 50. In the investigated pressure region (10^{-3} — 10^{-5} torr) a linear dependence between ion collector current and gas pressure was found.

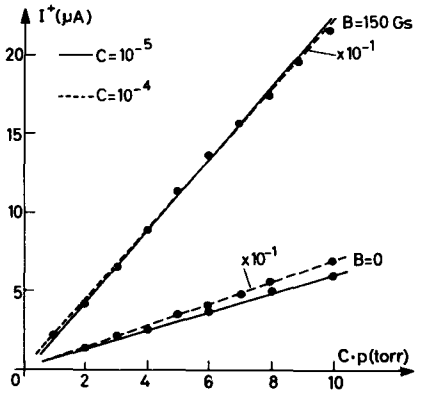

Fig. 50. Collector current vs. pressure.

Experiments have shown that the pumping action of the split-magnetron gauge can be controlled by the magnetic field. At magnetic fields higher than critical the pumping action is rather high, since the number of produced ions is increased and the ion collector surface is large.

4. CONCLUSION

The dynamics of intense electrical discharges in the gas magnetron diode has not been fully explored both theoretically and experimentally. The present-day knowledge of this subject is restricted to the low intensity cold cathode magnetron diode.

The aim of this thesis is to clarify theoretically and experimentally the mechanism of intense electrical discharge in the gas magnetron diode.

The results summarized in Chapter 1 indicate that the intense discharge is accompained with a dense electron cloud rotating around the cathode. Electron transit time measurements, which constitute an original method of investigation of the mechanism of the gas discharge in magnetron geometry, lead to the same conclusion. As the transit time with strong magnetic fields is about 10^4 times longer than that without a magnetic field, the electron transport is highly influenced by collisions. On the other hand, the tangential drift velocities are 100—10000 times larger than the radial velocity, and therefore we conclude that the tangential current can be of order of 1000 amperes if the anode current is of the order of 1 ampere. These diamagnetic currents create in the interior of the diode a magnetic field opposed to the external field B, which explains the anode current cutoff at magnetic fields higher than B_c.

These conclusions indicate that direct experimental determination of the magnetic field in the vicinity of the cathode can give a clear picture of magnetron discharge. Optical spectroscopy, based on Doppler shift, appears to be a natural means for investigation of the rotation of other plasma constituents with the electron cloud.

The pulse method of electron transit time measurement may be continued in two directions: firstly, spectroscopic analysis of the discharge can give the speed of the ionization wave from cathode to anode; secondly, it would be useful to analyze the extracted ion beam under pulsed conditions, as the expected pulsed current should exceed many times those obtainable in the dc regime.

Probe measurements indicate that the electron velocity distribution is Maxwellian even at low pressures. The relatively high electron concentration of 10^{11} cm^{-3} is related to the formation of an intense space charge cloud.

The noise spectrum emitted from the gas magnetron diode is characterized by strong coherent signals. The strong sinusoidal oscillations registered prove that, under certain circumstances, the rotating space cloud becomes unstable.

In Chapter 2 it was proved that, under the action of the magnetic field induced by the cathode heating current, the anode current can be cut off. It was also shown that such a field may influence the initiation of an electrical discharge very similar

to that existing in an external magnetic field. As all ion sources have a strong emitting filament, the influence of the filament magnetic field can be important in systems which are not cylindrical.

In Chapter 3, which deals with applications of the gas magnetron, it is shown that the magnetron ion sources has a number of advantages over other types of ion sources. In spite of its simple construction, this source yields strong singly and multiply charged ion beams of a large number of gaseous and metallic elements. Ions of refractory materials have been obtained in the magnetron ion source by exposing to cathode sputtering powders deposited directly on the filament. It was demonstrated that the magnetron diode can be successfully used as a miniature ion source for mass spectrometric purposes in the analysis of microgramme quantities of unknown substances.

A new type of ionization gauge has been developed. The high rate of ionization and the large collector surface hold promise of successful ion pump operation.

REFERENCES

[1] A.W. HULL, *The effect of a uniform magnetic filed on the motion of electrons between coaxial cylinders.* Phys. Rev. **18** (1921) 31.

[2] П. Л. КАПИЦА, *Электроника больших мощностей.* Москва, 1962.

[3] L. PAGE, N. I. ADAMS, *Space charge in cylindrical magnetron.* Phys. Rev. **69** (1946) 494.

[4] L. BRILLOUIN, F. BLOCH, *Electronic theory of the cylindrical magnetron.* Advances in Electronics, **3** (1951) 145—181.

[5] G. HOK, *A statistical approach to the space-charge distribution in a cut-off magnetron.* J. Appl. Phys. **23** (1952) 983.

[6] R. Q. TWISS, *On the steady-state theory of the magnetron.* Advances in Electronics, **5** (1953) 247—289.

[7] H. C. NEDDERMAN, *Space charge distribution in a static magnetron.* J. Appl. Phys. **26** (1955) 1420.

[8] М. Я. МИНЦ, *К теории магнетрона со сплошным анодом.* ЖТФ **27** (1957) 1306.

[9] М. Я. МИНЦ, *К теории магнетрона с разрезным анодом.* ЖТФ **27** (1957) 1313.

[10] Л. Э. ПАРГАМАНИК, М. Я. МИНЦ, *К диффузионной теории магнетрона (статический режим),* ЖТФ **27** (1957) 1301.

[11] P. A. LINDSAY, *General steady state theory of cylindrical magnetrons,* J. Electr. and Control **9** (1960) 241.

[12] J. COSTE, L. DAGENS, *Une théorie purement statique du magnétron,* J. Electr. and Control **14** (1963) 129.

[13] P. A. LINDSAY, G. D. SIMS, *Electron »temperature« in crossed fields,* J. Electr. and Control **14** (1963) 273.

[14] P. A. LINDSAY, R. S. GOODELL, *Velocity and potential distribution in a linear, smooth anode magnetron (magnetic diode).* J. Appl. Phys. **36** (1965) 411.

[15] K. MOUTHAAN, C. SÜSSKIND, *Anode current in the smooth-bore magnetron.* Proc. IEEE **54** (1966) 430.

[16] P. A. REDHEAD, *Oscillations in magnetically confined cold-cathode discharges at very low pressures.* Can. J. Phys. **43** (1965) 1001.

[17] G. B. COLLINS, *Microwave magnetrons.* MIT ser. **6** (1948).

[18] P. A. REDHEAD, *The magnetron gauge: a cold-cathode vacuum gauge.* Can. J. Phys. **37** (1959) 1260.

[19] J. M. LAFFERTY, *Hot-cathode magnetron ionization gauge for the measurement of ultra-high vacua.* J. Appl. Phys. **32** (1961) 424.

[20] P. A. REDHEAD, E. V. Kornelsen, J. P. Hobson, *Ultrahigh vacuum in small glass systems.* Can. J. Phys. **40** (1962) 1814.

[21] J. M. LAFFERTY, *Hot-cathode magnetron ionization gauge with an electron multiplier ion detector for the measurement of extreme ultra-high vacua.* Rev. Sci. Inst. **34** (1963) 467.

[22] F. L. TORNEY, F. FEAKES, *Pressure measurements below* 10^{-10} *Torr with Bayard-Alpert and magnetron gauges.* Rev. Sci. Instr. **34** (1963) 1041.

[23] O. BINEMAN, *Generation and amplification of waves in dense charge beams under crossed field.* Nature **165** (1950) 474.

[24] R. E. LUNDGREN, C. SUSSKIND and J. R. WOODYARD, *Applications of cold-cathode parallel field devices.* IRE Trans. on Electron. Devices **8** (1961) 489.

[25] W. D. GILL, E. KAY, *Efficient low pressure sputtering in a large inverted magnetron suitable for film synthesis.* Rev. Sci. Instr. **36** (1965) 277.

[26] S. N. VAN VOORHIS, J. B. KUPER, G. P. HARNWELL, *Proton source for atomic desintegration experiments.* Phys. Rev. **45** (1934) 492.

[27] O. LUHR, *A source of doubly ionized helium.* Phys. Rev. **49** (1936) 317.

[28] М. М. Ситников, *Теория ионного тока в магнетроне применительно к источнику ионов.* I часть: ЖТФ **8** (1938) 1433; II часть: ЖТФ **8** (1938) 1527.

[29] И. М. Вигдорчик, *Получение больших ионных токов с помощью газомагнетрона.* ЖТФ **8** (1938) 1197.

[30] B. PEROVIĆ, *Direct current magnetron as ion source for gases and solids.* Proc. III Inter. Conf. Phen. in Ion. Gases, Venezia 1957, p. 813.

[31] Л. А. Арцимович, *Управляемые термоядерние реакции.* Москва, 1961.

[32] B. A. TOZER, *Rotating plasma.* Proc. IEE **112** (1965) 218.

[33] E. P. BAUBIAN, C. E. RASMUSSEN, J. KISTEMAKER, *Ionization and current growth in an $E \times B$ discharge.* Proc. VIII Inter. Conf. Phen. in Ion. Gases, Vienna 1967, p. 176.

[34] D. TOŠIĆ, B. ČOBIĆ, B. PEROVIĆ, *Ispitivanje gasnog pražnjenja u ukrštenim električnim i magnetskim poljima.* I jugosl. simpozijum o fizici jonizovanog gasa, Beograd 1962.

[35] B. ČOBIĆ, D. TOŠIĆ, B. PEROVIĆ, *An intense magnetron ion source for high-melting point materials.* Nucl. Instr. and Methods **24** (1963) 358 .

[36] B. ČOBIĆ, D. TOŠIĆ, B. PEROVIĆ, *Aston bands in the electromagnetic mass separator.* Nucl. Instr. and Methods **25** (1963) 157.

[37] Z. JURELA, I. TERZIĆ, D. TOŠIĆ, *Ispitivanje gasnog pražnjenja u jednosmernom cilindričnom magnetronu sa unutrašnjom katodom u oblasti cutoff*-a. IBK int. publ. 131 (1964).

[38] D. TOŠIĆ, *The appearance of the self cuf-off phenomenon in the cylindrical diode.* J. Electr. and Control **17** (1964) 623.

[39] D. TOŠIĆ, *Jedna nova modifikacija magnetronskih merača vakuuma.* IBK int. publ. 122 (1964).

[40] D. TOŠIĆ, *Cut-off phenomena in the magnetron ion source.* Nucl. Instr. and Methods **38** (1965) 26.

[41] D. TOŠIĆ, B. STANIĆ, *The oscillations in the dc magnetron gas discharge.* Proc. VII Intern. Conf. Phen. in Ion. Gases, Beograd 1965, vol. 1, p. 527.

[42] B. ČOBIĆ, B. PEROVIĆ, D. TOŠIĆ, *A new mass spectrometer ion source for solids.* J. Sci. Instr. **36** (1965) 1844.

[43] D. TOŠIĆ, B. ČOBIĆ, *High sensitive dc split-magnetron ionization gauge.* Trans. of the Third Intern. Vacuum Congress, Stuttgart 1965, vol 2, p. 497.

[44] D. TOŠIĆ, *Karakteristike paljenja pražnjenja u jednosmernom cilindričnom magnetronu na niskom pritisku.* IBK int. publ. 475 (1966).

[45] D. TOŠIĆ, *Jednosmerni cilindrični magnetron kao naponski filter.* Zbornik radova XI konf ETAN, Niš 1967, p. 303.

[46] D. TOŠIĆ, V. MILJEVIĆ, *Low-pressure discharge in the magnetron diode.* Proc. VIII Intern. Conf. Phen. in Ion. Gases, Vienna 1967, p. 183.

[47] D. TOŠIĆ, *Transport elektrona u gasnoj magnetronskoj diodi.* IBK int. publ. 588 (1967).

[48] D. GABOR, *Stationary electron swarms in electromagnetic fields.* Proc. Roy. Soc. (London) A **183** (1945) 436.

[49] И. И. Вассерман, *Вращающийся пространственный заряд в магнетроне со сплошным анодом.* ЖТФ **18** (1948) 785.

[50] A. GUTHRIE, R. K. WAKERLING, eds., *The characteristics of electrical discharges in magnetic fields.* New York, 1949.

[51] M. HOYAUX, R. LEMAITRE, P. GANS, *Theory and probe measurements in a magnetic ion source.* J. Appl. Phys. **26** (1955) 110.

[52] G. DUMAS, *Étide de la resonance gyromagnétique dans la gauge de Penning.* Rev. gen. d'elec. **64** (1955) 331.

[53] W. HONIG, P. PARZEN, *A gas discharge noise source.* IRE Conv. Rec. **3** — Pt. 3 (1955) 3

[54] J. C. HELMER, R. L. JEPSEN, *Electrical characteristics of a Penning discharge.* Proc. IRE (1961) 1920.

[55] W. KNAUER, *Mechanism of the Penning discharge at low pressures.* J. Appl. Phys. **33** (1962) 2093.

[56] R. H. LEVY, *Diocotron instability in a cylindrical geometry.* Phys. Fluids **8** (1965) 1288.

[57] J. P. HOBSON, P.A. REDHEAD, *Operation of an inverted-magnetron gauge in the pressure range* 10^{-3} *to* 10^{-12} mmHg. Can. J. Phys. **36** (1958) 271.

[58] М. Г. КАГАНСКИЙ, Д. Л. КАМИНСКИЙ, А. Н. КЛЮЧАРЕВ, *Когерентные колебания в высоковольтном разряде Пеннинга.* ЖТФ **34** (1964) 1050.

[59] W. KNAUER, *Diocotron instability in plasmas and gas discharges.* J. Appl. Phys. **37** (1966) 602.

[60] D. G. DOW, *Electron-beam probing of a Penning discharge.* J. Appl. Phys. **34** (1963) 2395.

[61] P. A. REDHEAD, *The Townsend discharge in a coaxial diode with axial magnetic field.* Can. J. Phys. **36** (1958) 255.

[62] M. J. BERNSTEIN, *Electron drift and diffusion measurements in* H_2 *and* D_2 *with crossed electric and strong magnetic fields.* Phys. Rev. **127** (1962) 335.

[63] S. C. HAYDON and A. G. ROBERTSON, *The effective collision frequency in molecular hydrogen in the presence of a transverse magnetic field.* Proc. Phys. Soc. **82** (1963) 343.

[64] O. D. OLSON and H. M. SKARSGARD, *The diffusion of a highly ionized plasma across a magnetic field.* Can. J. Phys. **43** (1965) 855.

[65] K. MOUTHAAN and C. SÜSSKIND, *Statistical theory of electron transport in the smooth-bore magnetron.* J. Appl. Phys. **37** (1966) 2598.

[66] W. B. KUNKEL and A. R. SHERWOOD, *Formative time of crossed-field breakdown.* Proc. VIII Intern. Conf. Phen. in Ion. Gases, Vienna 1967, p. 177.

[67] M. R. BHIDAY, A. S. PAINHANKAR, B. L. SHARDA, *Collision frequency in air with crossed electric and magnetic fields.* Brit. J. Appl. Phys. **18** (1967) 241.

[68] Е. Т. КУЧЕРЕНКО, О. К. НАЗАРЕНКО, *Особенности разряда в магнитном поле с колебанием электронов.* Радиотехника и Электроника **4** (1959) 1253.

[69] E. H. HIRSCH, *Excess energy electrons.* Br. J. Appl. Phys. **15** (1964) 909.

[70] Е. Т. КУЧЕРЕНКО, В. П. ИГНАТКО, *Об одной форме затрудненного разряда в магнитном поле.* Радиотехника и Электроника **9** (1964) 177.

[71] М. М. БУТУСОВ, С. А. ФРИДРИХОВ, *Об аномальном нарушении хэлловского условиа отсечки в сильных скрещенных полях.* ЖТФ **34** (1964) 288.

[72] E. H. HIRSCH, *Cut-off characteristics of a cylindrical magnetron.* Int. J. Electron. **21** (1967) 521.

[73] E. H. HIRSCH, *Modification of magnetron cut-off characteristics by the introduction of positive ions.* Int. J. Electron. **22** (1967) 215.

[74] I. ŠEVARAC, B. PEROVIĆ, B. DUNJIĆ, R. PROTIĆ, 60° *sector type electromagnetic isotope separator in the Institute of nuclear sciences — Belgrade.* Nucl. Instr. and Methods **3** (1958) 245.

[75] E. L. CHAFFEE, *Theory of thermionic vacuum tubes.* New York 1933.

SADRŽAJ RADA

DINAMIKA ELEKTRIČNOG PRAŽNJENJA U GASNOJ MAGNETRONSKOJ DIODI

Dobrilo Đ. Tošić

Električno pražnjenje u gasnoj magnetronskoj diodi u potpunosti se razlikuje od pražnjenja u običnoj gasnoj diodi. Aksijalno magnetsko polje produžuje putanje elektrona, što uslovljava intenzivniju jonizaciju gasa, tako da se može realizovati intenzivno pražnjenje i na niskom pritisku. Ovaj rad preduzet je u cilju proučavanja niza pojava koje se dešavaju u gasnoj magnetronskoj diodi, kao i mogućnosti njene primene.

U prvom delu disertacije *Karakteristike gasne magnetronske diode* date su osobine ove diode vezane uglavnom za osnovno svojstvo magnetronske diode — prekid anodne struje (cutoff). Pokazano je da se u gasnoj magnetronskoj diodi anodna struja prekida na mnogo jačim magnetskim poljima, nego što je to slučaj u vakuumskoj diodi. Na magnetskom polju slabijem od kritičnog magnetskog polja B_c, koje odgovara cutoff-u, gasna magnetronska dioda ponaša se kao dioda na koju nije primenjeno magnetsko polje. Međutim, ako se magnetsko polje neznatno poveća iznad B_c, anodna struja se nekoliko puta povećava. Sa daljim porastom magnetskog polja do prekida anodne struje dolazi na magnetskim poljima za red veličine jačim od B_c. Ovakvo ponašanje gasne magnetronske diode može se pripisati pojavi sekundarnih elektrona, koji nastaju u sudarima primarnih elektrona sa neutralnim atomima gasa.

Teorijska analiza dinamike kretanja elektrona pokazuje da se jedan elektron na putu od katode do anode u uslovima niskog pritiska sudari $4(B/B_c)^2$ puta, što znači da se sa porastom magnetskog polja naglo povećava broj sudara, tj. jonizacija gasa. S druge strane, energija elektrona se smanjuje, tako da se na jednoj kritičnoj vrednosti magnetskog polja pražnjenje prekida.

Pored standardnih statičkih karakteristika gasne magnetronske diode, dati su rezultati merenja temperature i koncentracije elektrona u intenzivnom magnetronskom pražnjenju. Pokazano je da i pored niskog pritiska gasa i malih dimenzija diode zahvaljujući dejstvu magnetskog polja dolazi do termalizacije plazme, tako da se dobija Maxwellova raspodela brzina elektrona.

U režimu rada magnetronske diode kada je pražnjenje prekinuto uočene su snažne koherentne oscilacije reda 0,5—1 MHz, koje su pripisane egzistenciji intenzivnog rotirajućeg elektronskog oblaka. Ispitana je promena učestanosti ovih oscilacija sa magnetskim poljem, anodnim naponom i pritiskom gasa.

Teorijski i eksperimentalno studiran je problem transporta elektrona u gasnoj magnetronskoj diodi. Pokazano je da je vreme transporta elektrona od katode do anode srazmerno B^3, a obrnuto srazmerno pritisku gasa. Primenom impulsnog anodnog napona razvijena je metoda merenja ovog vremena. Rezultati pokazuju da se i pored svih aproksimacija i ograničenja pod kojima je izvedena teorijska formula, eksperimentalni rezultati dobro slažu.

U drugom delu disertacije *O problemu sopstvenog polja* proučavan je uticaj struje grejanja katode na karakteristike magnetronske diode. Kod snažne magnetronske diode upotrebljavaju se direktno grejane katode sa visokom emisionom moći, tako da struje grejanja katode idu i do nekoliko desetina ampera. U toku merenja uočena je pojava da sa povećanjem grejanja katode može doći do prekida anodne struje (tzv. sopstveni cutoff), što je pripisano dejstvu magnetskog polja indukovanog strujom grejanja. Ova pojava nije do sada eksperimentalno zapažena, s obzirom da se kod klasičnih dioda upotrebljavaju ili indirektno grejane katode ili direktno grejane katode sa relativno slabim strujama.

Izvedena je zavisnost pojave sopstvenog cutoff-a od dimenzija diode, kao i uticaj naizmeničnog sopstvenog magnetskog polja na širenje osnovne cutoff karakteristike, koja daje vezu između anode struje i aksijalnog magnetskog polja. Pokazano je da naizmenično sopstveno magnetsko polje najviše doprinosi širenju cutoff karakteristike.

S obzirom da je sopstveno magnetsko polje ortogonalno na električno polje, uočeno je da gasno pražnjenje u ovim poljima ima osobine analogne pražnjenju pod dejstvom aksijalnog magnetskog polja. Na osnovu merenja ekstrahovanog jonskog snopa iz magnetronskog izvora utvrđeno je da se jonski snop može modulisati strujom grejanja katode.

U trećem delu *Primene gasne magnetronske diode* dati su samo neki primeri upotrebe magnetronske diode. Glavna pažnja posvećena je magnetronskom jonskom izvoru i njegovim osobinama. Na osnovu iznetih rezultata u prvom delu disertacije, jasno proizilazi zaključak da se gasna magnetronska dioda, zbog specifičnog dejstva magnetskog polja, može uspešno upotrebiti kao intenzivni jonski izvor. Veoma duge putanje elektrona dovode do efikasne jonizacije gasa. Ovaj jonski izvor ima niz prednosti nad ostalim izvorima: Jednostavna konstrukcija, intenzivni ekstrahovani jonski snop, visok prinos višestruko naelektrisanih jona, dobijanje jonskih snopova široke skale elemenata uz relativno malu uloženu energiju.

Zahvaljući specifičnoj geometriji magnetronskog izvora razvijen je novi metod za dobijanje jona visokotopljivih elemenata, koji se sastoji u fiksiranju praha odgovarajućeg elementa na katodu. Ovaj metod je proveren na nizu elemenata, čije temperature topljenja idu do 3000°C.

Opisan je metod analize sastava jonskog snopa iz magnetronskog jonskog izvora pomoću elektromagnetske analize izotopa. Izneti su rezultati merenja količine višestruko naelektrisanih jona, uzimajući u obzir tzv. Astonove mesene spektre, koji nastaju kao posledica interakcije primarnog jonskog snopa sa atomima rezidualnog gasa u analizatoru elektromagnetskog separatora izotopa.

Magnetronska dioda uspešno je primenjena na konstrukciju minijaturnog jonskog izvora za masenu analizu sastava nepoznatih supstanci. Metod fiksiranja metalnog praha na katodu omogućio je da se dobiju dovoljni jonski snopovi miligramskih količina polaznog materijala. Primenom zakočnog i skretnog potencijala

dokazano je da magnetronski jonski izvor daje jonski snop sa uskim spektrom energija, što predstavlja najvažniji kriterijum za primenljivost ovog izvora u masenoj spektrometriji.

Na kraju ovog dela izneta je jedna nova modifikacija magnetronskih merača vakuuma. U tu svrhu upotrebljena je magnetronska dioda sa rascepljenom anodom, tako da jedan deo predstavlja elektronski, a drugi jonski kolektor. Pokazano je da ovakva jonizaciona cev ima linearne karakteristike sa daleko većim koeficijentom osetljivosti, čime je opravdana njena upotreba u tehnici merenja visokog vakuuma.

* * *

Autor izražava veliku zahvalnost Prof. B. Đ. Perović za višegodišnju saradnju i niz korisnih diskusija i sugestija, Prof. B. V. Surutki i Prof. D. S. Mitrinoviću za stalni interes za ovaj rad, D. B. Iliću, Dr B. A. Aničinu i Dr R. R. Janiću za pomoć u pripremanju rukopisa.